Journal of Computational Physics 480 (2023) 112034

Contents lists available at ScienceDirect

Journal of Computational Physics

journal homepage: www.elsevier.com/locate/jcp

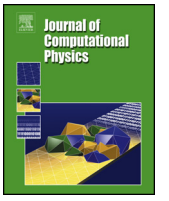

Bound/positivity preserving SAV schemes for the Patlak-Keller-Segel-Navier-Stokes system ☆

Xueling Huang [a], Jie Shen [a,b,*]

[a] School of Mathematical Sciences and Fujian Provincial Key Laboratory on Mathematical Modeling and High Performance Scientific Computing, Xiamen University, Xiamen, Fujian, 361005, China
[b] Department of Mathematics, Purdue University, West Lafayette, IN 47907, USA

ARTICLE INFO

Article history:
Received 18 September 2022
Received in revised form 15 February 2023
Accepted 19 February 2023
Available online 24 February 2023

Keywords:
Patlak-Keller-Segel-Navier-Stokes equations
Bound/positivity preserving
Energy dissipation
Relaxed SAV method

ABSTRACT

The Patlak-Keller-Segel-Navier-Stokes system describes the biological chemotaxis phenomenon in the fluid environment. It is a coupled nonlinear system with unknowns being the cell density, the concentration of chemoattractants, the fluid velocity and the pressure, and it satisfies an energy dissipation law, preserves the bound/positivity and mass of the cell density. We develop in this paper a class of scalar auxiliary variable (SAV) schemes with relaxation which preserve these properties unconditionally at the discrete level, and only require solving decoupled linear systems with constant coefficients at each time step. We present ample numerical results to validate these schemes, simulate the chemotactic non-aggregation and aggregation with a saturation concentration, as well as investigate the blow-up phenomenon.

1. Introduction

The biological chemotaxis phenomenon refers to the directional movement of cells along the concentration gradient of the chemoattractant in their tissues or living environments. To describe this phenomenon, many mathematical models have been proposed [2,16,21]. Among these models, the Patlak-Keller-Segel-Navier-Stokes (PKS-NS) model, firstly introduced by [14], couples the parabolic-elliptic Patlak-Keller-Segel (PKS) equations describing the interaction between cells and chemoattractant [30,37], and the well-known incompressible Navier-Stokes (NS) equations controlling the motion of the fluid [40]. It indicates that cells and chemoattractant are transported by the fluid in their living environment when cells move towards the direction of high concentration of the chemoattractant, while the motion of fluid is further affected by a friction force on the moving cells.

It is known that, if the fluid transport structure is introduced in the cell density evolution equation, the classical free energy will no longer decay in general. This causes a major difficulty in analyzing the classical coupled chemotaxis-fluid model, proposed by Hillesdon et al. [22] and Tuval et al. [41]. Some theoretical results on the existence and uniqueness of solutions for the classical chemotaxis-fluid model are presented in [7,28,32,44]. On the other hand, the PKS-NS system that we consider in this paper inherits the energy dissipation of the classical PKS system, and some analytical results for the PKS-NS model are available. For examples, Gong and He [14] first proved that, if the total mass of cells M_ρ is strictly less

☆ This work is supported in part by NSFC 11971407.
* Corresponding author at: Department of Mathematics, Purdue University, West Lafayette, IN 47907, USA.
E-mail addresses: hxlmath@163.com (X. Huang), shen7@purdue.edu (J. Shen).

https://doi.org/10.1016/j.jcp.2023.112034
0021-9991/

than 8π, then classical solutions exist for any finite time and their H^s norms are almost uniformly bounded in time. Later, Lai et al. [35] analyzed the global existence of the PKS-NS system with critical and subcritical mass, and pointed out that the positivity of cell density is a direct consequence of the strong maximum principle.

It is worth mentioning that the aggregation can lead to blow-up for the two-dimensional PKS equations once M_ρ exceeds a threshold [4,16,27,36]. Here the blow-up, which does not occur in reality, means that the concentration reaches several orders of magnitude larger and is beyond the range that the model can describe. An interesting and important question is how the fluid coupling can change the blow-up behavior. Numerical evidence in [33] indicates that solutions to a parabolic-elliptic PKS-Stokes model exist for initial mass $M_\rho \approx 27$, which is larger than 8π (the critical mass for the system without fluid), but for even larger mass $M_\rho \approx 40$, blow-up seems to occur. Lorz [33] pointed out that the blow-up could be delayed when the PKS system is coupled with fluids. By analyzing the PKS equations with an additional advection term modeling ambient fluid flow, Kiselev and Xu [31] indicated that the fluid flow might suppress the potential chemotactic blow-up. Suppression of explosion in parabolic-elliptic and parabolic-parabolic PKS system via shear flows was proved in [5,17]. Despite of the known analytical results on blow-up suppression, finite-time blow-up of the PKS-NS system is still possible. For the Keller-Segel system coupled with the Navier-Stokes fluid, finite time blow-up criterion was analyzed in [29]. But for the PKS-NS system that we studied in this paper, it is unclear if solutions exist globally or blow up in finite time with $M_\rho > 8\pi$.

Compared with analytical works, the PKS-NS system is less studied numerically. There are two main difficulties to construct suitable numerical schemes: one is to preserve, at the discrete level, essential properties of the PKS-NS system which are mainly inherited from the PKS equations, including the bound/positivity preservation [6,12,20,42,43], energy dissipation and mass conservation [16,21,23,39]; the other is to efficiently deal with the strong nonlinear coupling for the fluid flow. Most existing methods mainly focus on the positivity preserving with a particular spatial discretization and usually lead to strict CFL restrictions on the time step [8,10,11,19,34]. Although there exist some unconditionally positivity-preserving schemes for the KS equations, such as the linear finite-volume scheme in combination with the upwind technique for KS equations in [47], it can only achieve first-order accuracy both in time and space, see also [1] for a nonlinear finite-volume-based scheme with the upwind technique; Shen and Xu [39] constructed numerical schemes for the classical and modified KS systems with a gradient flow structure by rewriting the term $\Delta\rho$ as $\nabla\cdot(\frac{\nabla f'(\rho)}{f''(\rho)})$, where $f''(\rho)=\frac{1}{\eta(\rho)}$, however, the energy stability is proved only for the first-order scheme, see [9] for a related work; a new class of bound/positivity preserving and energy stable schemes by combining SAV approach and the function transform approach were proposed in [23] for KS equations.

On the other hand, to deal with the strong nonlinear coupling for the fluid flow in the classical chemotaxis-fluid model, the vorticity formulation was used in [8] and [13]; a particle method combining with the finite volume method based on semi-implicit pressure was proposed in [18]; an operator splitting-type NS solver was used in [34] and the pressure-correction scheme was used in [19]. However, almost exclusively these schemes are restricted to first- or second-order accuracy in time. Very recently, Huang and Shen [24] constructed high-order semi-discrete-in-time and fully discrete (with Fourier-Galerkin in space) schemes for the incompressible NS equations with periodic boundary conditions, and carried out corresponding error analysis. Furthermore, this method was generalized to the non-periodic boundary conditions [45] in combination with consistent splitting schemes [15].

A main purpose of this paper is to construct a class of fully decoupled, bound/positivity preserving schemes for the PKS-NS system by combining the distinctive advantages of the methods presented in [23,24,26,45,48]:

- For the bound/positivity preservation, energy dissipation and mass conservation, we employ the approach in [23]. Namely, a suitable function transform is proposed first to keep the bound/positivity of the density solution, and then the generalized SAV approach is adopted to retain the energy dissipation and mass conservation. Different from the SAV scheme in [23,25], we introduce a relaxation factor to penalize the numerical error of the auxiliary variable [26,46,48]. This makes its modified energy closer to the original energy and improves its accuracy further.
- For the strong nonlinear coupling, we construct high-order semi-implicit SAV schemes based on the k-th order BDF-Adams-Bashforth schemes as in [24,45]. In the case of periodic boundary conditions, the pressure can be explicitly expressed as a function of the velocity so the method in [24,25] can be applied directly for the NS part. For non-periodic boundary conditions, we employ the consistent splitting approach and generalized semi-implicit SAV schemes as in [45].

The resultant schemes are totally decoupled, only requiring to solve a sequence of linear equations with constant coefficients, can be high-order in time and preserve essential properties of PKS-NS system.

Another main purpose of this paper is to use the proposed schemes to numerically investigate if solutions to the PKS-NS system exist globally or would blow up in finite time when $M_\rho > 8\pi$.

The rest of paper is organized as follows. In Section 2, we introduce the PKS-NS system and state some basic properties. In Section 3, a class of bound/positivity preserving generalized SAV schemes with relaxation (R-GSAV) are proposed in detail. Firstly, function transform for the PKS part of the system are proposed, and then decoupling techniques for the NS part are presented, followed by the fully decoupled R-GSAV scheme. Moreover, we show that these schemes enjoy bound/positivity preservation, unconditionally energy dissipation and mass conservation. Next, we validate these properties and the accuracy of the proposed scheme, simulate the chemotactic non-aggregation and aggregation with a saturation concentration, as well

as study the blow-up phenomenon by a series of numerical tests in Section 4. We end the paper with some concluding remarks in Section 5.

2. The PKS-NS system

We consider the following PKS-NS system:

$$\frac{\partial \rho}{\partial t} + \boldsymbol{u}\cdot\nabla\rho = \Delta\rho - \nabla\cdot\big(\eta(\rho)\nabla c\big), \tag{2.1}$$

$$-\Delta c = -\alpha c + \rho, \tag{2.2}$$

$$\frac{\partial \boldsymbol{u}}{\partial t} + \boldsymbol{u}\cdot\nabla\boldsymbol{u} + \nabla p = \nu\Delta\boldsymbol{u} + \rho\nabla c, \tag{2.3}$$

$$\nabla\cdot\boldsymbol{u} = 0, \tag{2.4}$$

with initial conditions

$$\rho|_{t=0} = \rho_0, \quad \boldsymbol{u}|_{t=0} = \boldsymbol{u}_0, \tag{2.5}$$

in a bounded domain $\Omega \subset \mathbf{R}^2$ and a time interval $[0, T]$ with a finite time T, and with either

- periodic boundary conditions for all quantities; or
- the no-flux boundary condition for the cell density ρ, the homogeneous Neumann boundary condition for the concentration of chemoattractants c, and the no-slip boundary condition for the fluid velocity $\boldsymbol{u}$:

$$\frac{\partial \rho}{\partial \boldsymbol{n}} - \eta(\rho)\frac{\partial c}{\partial \boldsymbol{n}} = 0, \quad \frac{\partial c}{\partial \boldsymbol{n}} = 0, \quad \boldsymbol{u} = \boldsymbol{0}, \quad \text{on } \partial\Omega, \tag{2.6}$$

where $\boldsymbol{n}$ is the outward unit-normal to the boundary $\partial\Omega$.

The function $\eta(\rho) \geq 0$ describes the concentration-dependent mobility. It is a smooth function with $\eta(0) = 0$. The coefficient $\alpha \geq 0$ represents the consumption rate of the chemoattractant. Note that when $\alpha = 0$, the equation (2.2) should be adjusted as $-\Delta c = \rho - \langle\rho\rangle$ with $\langle\rho\rangle = \frac{1}{|\Omega|}\int_\Omega \rho dx$, due to the compatibility with the boundary conditions involved [14,27,33,36]. The first two equations are the PKS equations with a transport term due to the fluid velocity, in which the first equation reveals the time evolution of the cell density subjected to aggregation induced by chemoattractant c, diffusion caused by random Brownian motion, and transportation by fluid flow $\boldsymbol{u}$, while the second equation describes the connection between the cell density ρ and the chemoattractant c. The last two equations are the Navier-Stokes equations with viscosity coefficient ν and a friction force $\rho\nabla c$ on the moving cells and reaction forces act on the fluid [14].

It can be easily shown (see below) that PKS-NS system is dissipative with the following free energy

$$E_{tot}(\rho, c, \boldsymbol{u}) = \int_\Omega \left(f(\rho) - \rho c + \frac{1}{2}|\nabla c|^2 + \frac{\alpha}{2}c^2 + \frac{1}{2}|\boldsymbol{u}|^2 \right) dx \tag{2.7}$$

where the function $f(\rho)$ is determined from $f''(\rho) = \frac{1}{\eta(\rho)}$.

Several typical choices of $\eta(\rho)$ and the corresponding function $f(\rho)$ are as follows:

1. The classical PKS-NS system: $\eta(\rho) = \rho$. We can choose $f(\rho) = \rho\log\rho - \rho$ with $\rho \in (0, +\infty)$ [35].
2. The PKS-NS system with a bounded mobility: $\eta(\rho) = \frac{\rho}{1+\kappa\rho}$ $(\kappa > 0)$ [42,43]. In this case, we set $f(\rho) = \rho\log\rho - \rho + \frac{\kappa}{2}\rho^2$ with $\rho \in (0, +\infty)$.
3. The PKS-NS system with a saturation concentration: $\eta(\rho) = \rho(1 - \frac{\rho}{M})$, here $M > 0$ is the saturation concentration, and the mobility tends to zero when it is near saturation [12,20]. We can set $f(\rho) = \rho\log\rho + (M - \rho)\log(1 - \frac{\rho}{M})$ with $\rho \in (0, M)$.

Hence, the density solution ρ of the PKS-NS system is positivity preserving in Cases 1 and 2, and bound preserving in Case 3.

Using the identity $\Delta\rho = \nabla\cdot(\frac{1}{f''(\rho)}\nabla f'(\rho))$, we can rewrite (2.1)-(2.2) as a gradient flow about ρ and c with an extra transport term:

$$\frac{\partial \rho}{\partial t} + \boldsymbol{u}\cdot\nabla\rho = \nabla\cdot\left(\frac{1}{f''(\rho)}\nabla(f'(\rho) - c)\right) = \nabla\cdot\left(\eta(\rho)\nabla\frac{\delta E_{tot}}{\delta\rho}\right), \tag{2.8}$$

$$0 = -\Delta c + \alpha c - \rho = \frac{\delta E_{tot}}{\delta c}. \tag{2.9}$$

Taking the inner products of (2.8) with $\frac{\delta E_{tot}}{\delta \rho} = f'(\rho) - c$ and of (2.3) with $\frac{\delta E_{tot}}{\delta \boldsymbol{u}} = \boldsymbol{u}$, integrating by parts, thanks to $\nabla \cdot \boldsymbol{u} = 0$, we find

$$(\frac{\partial \rho}{\partial t}, \frac{\delta E_{tot}}{\delta \rho}) = -\int_{\Omega} \eta(\rho) |\nabla \frac{\delta E_{tot}}{\delta \rho}|^2 dx - (\boldsymbol{u} \cdot \nabla c, \rho), \tag{2.10}$$

$$(\frac{\partial \boldsymbol{u}}{\partial t}, \frac{\delta E_{tot}}{\delta \boldsymbol{u}}) = -\int_{\Omega} \nu |\nabla \boldsymbol{u}|^2 dx + (\rho \nabla c, \boldsymbol{u}). \tag{2.11}$$

Summing up equations (2.10) and (2.11), we immediately obtain the energy dissipative law

$$\frac{dE_{tot}(\rho, c, \boldsymbol{u})}{dt} = -\int_{\Omega} \left(\eta(\rho) |\nabla \frac{\delta E_{tot}}{\delta \rho}|^2 + \nu |\nabla \boldsymbol{u}|^2 \right) dx. \tag{2.12}$$

Integrating (2.1) over Ω, we deduce that

$$\frac{d}{dt} \int_{\Omega} \rho dx = 0. \tag{2.13}$$

Remark 2.1. We note that the PKS-NS system with $\boldsymbol{u} \equiv \boldsymbol{0}$ reduces to the classical PKS model. In Case 1, i.e., $\eta(\rho) = \rho$, it is known that the density ρ of two-dimensional PKS model can blow up in finite time if the initial mass M_ρ exceeds a threshold [16,27,36].

3. Bound/positivity preserving R-GSAV schemes

We first use a suitable function transform for the cell density so that the bound or positivity of the cell density can always be preserved, and then describe decoupling techniques for the NS part, followed by constructing fully decoupled R-GSAV schemes which enjoy following properties: the bound/positivity preservation, unconditionally energy dissipation and mass conservation.

3.1. Function transform for the cell density ρ

For preserving positivity in Cases 1 and 2, we set

$$\rho = \exp(v). \tag{3.1}$$

Substituting the above into (2.1), we get

$$\frac{\partial v}{\partial t} + \boldsymbol{u} \cdot \nabla v = \Delta v + |\nabla v|^2 - \frac{1}{\exp(v)} \nabla \cdot (\eta(\rho) \nabla c). \tag{3.2}$$

For preserving the bound $(0, M)$ in Case 3, we use the function transform

$$\rho = \frac{M}{2} \tanh(v) + \frac{M}{2}. \tag{3.3}$$

Substituting this transform into (2.1), we obtain

$$\frac{\partial v}{\partial t} + \boldsymbol{u} \cdot \nabla v = \Delta v + \frac{\tanh''(v)}{\tanh'(v)} |\nabla v|^2 - \frac{2}{M \tanh'(v)} \nabla \cdot (\eta(\rho) \nabla c). \tag{3.4}$$

3.2. Decoupling techniques for the velocity $\boldsymbol{u}$ and pressure p

Since the NS equations with different boundary conditions require different decoupling techniques for the velocity $\boldsymbol{u}$ and pressure p, we consider periodic boundary conditions and non-periodic boundary conditions, respectively.

For periodic boundary conditions, we can explicitly eliminate the pressure as follows. Taking the divergence on both sides of (2.3) and (2.4), we have

$$-\Delta p = \nabla \cdot (\boldsymbol{u} \cdot \nabla \boldsymbol{u} - \rho \nabla c), \tag{3.5}$$

$$\nabla p = -(\boldsymbol{u} \cdot \nabla \boldsymbol{u} - \rho \nabla c) - A(\boldsymbol{u} \cdot \nabla \boldsymbol{u} - \rho \nabla c), \tag{3.6}$$

where A is a linear operator in $L_0^2(\Omega) := \{v \in L^2(\Omega) : \int_\Omega v dx = 0\}$ defined by

$$Av := \nabla \times \nabla \times \Delta^{-1} v, \quad \forall v \in L_0^2(\Omega). \tag{3.7}$$

Hence equations (2.3) and (2.4) reduce to

$$\frac{\partial \boldsymbol{u}}{\partial t} = \nu \Delta \boldsymbol{u} + A\left(\boldsymbol{u} \cdot \nabla \boldsymbol{u} - \rho \nabla c\right). \tag{3.8}$$

Therefore, we can obtain the velocity $\boldsymbol{u}$ from (3.8) and the pressure p from (3.5).

In the case of non-periodic boundary conditions, we adopt the consistent splitting approach [15,45] which is based on replacing the divergence free condition (2.4) by the following pressure-Poisson equation in the weak form

$$\begin{aligned}(\nabla p, \nabla q) &= (\nu \Delta \boldsymbol{u} - \boldsymbol{u} \cdot \nabla \boldsymbol{u} + \rho \nabla c, \nabla q) \\ &= (-\nu \nabla \times \nabla \times \boldsymbol{u} - \boldsymbol{u} \cdot \nabla \boldsymbol{u} + \rho \nabla c, \nabla q), \quad \forall q \in H^1(\Omega).\end{aligned} \tag{3.9}$$

Then, we can decouple the velocity $\boldsymbol{u}$ and pressure p by semi-implicit schemes for equations (2.3) and (3.9) described in the next subsection.

3.3. Fully decoupled R-GSAV schemes

To avoid repetition, we present the schemes for the PKS-NS system with non-periodic boundary conditions (2.6). The case of periodic boundary condition is much simpler and can be dealt with similarly.

To fix the idea, we consider positivity preserving, i.e., $\eta(\rho) = \rho$, the case of bound preserving can be treated similarly. In this case, $f(\rho) = \rho \log(\rho) - \rho$ is strictly convex and $E_{tot}(\rho, c, \boldsymbol{u})$ is bounded from below. Hence, there exists $C_0 > 0$ such that $E(\rho, c, \boldsymbol{u}) := E_{tot}(\rho, c, \boldsymbol{u}) + C_0 \geq 1$. Following the paper [25], we introduce a SAV

$$r(t) = E(\rho, c, \boldsymbol{u}), \tag{3.10}$$

after applying the function transform (3.1) for the cell density ρ, then we expand the PKS-NS system as

$$\frac{\partial v}{\partial t} + \boldsymbol{u} \cdot \nabla v = \Delta v + |\nabla v|^2 - \frac{1}{\exp(v)} \nabla \cdot (\eta(\rho) \nabla c), \tag{3.11}$$

$$-\Delta c = -\alpha c + \rho, \tag{3.12}$$

$$\frac{\partial \boldsymbol{u}}{\partial t} + \boldsymbol{u} \cdot \nabla \boldsymbol{u} + \nabla p = \nu \Delta \boldsymbol{u} + \rho \nabla c, \tag{3.13}$$

$$\frac{dr}{dt} = -\frac{r}{E(\rho, c, \boldsymbol{u})} G(\rho, c, \boldsymbol{u}), \tag{3.14}$$

$$(\nabla p, \nabla q) = (-\nu \nabla \times \nabla \times \boldsymbol{u} - \boldsymbol{u} \cdot \nabla \boldsymbol{u} + \rho \nabla c, \nabla q), \quad \forall q \in H^1(\Omega), \tag{3.15}$$

where $G(\rho, c, \boldsymbol{u}) = \int_\Omega \left(\eta(\rho) |\nabla \frac{\delta E_{tot}}{\delta \rho}|^2 + \nu |\nabla \boldsymbol{u}|^2\right) dx \geq 0$, and the boundary conditions are

$$\exp(v) \frac{\partial v}{\partial \boldsymbol{n}} - \eta(\rho) \frac{\partial c}{\partial \boldsymbol{n}} = 0, \quad \frac{\partial c}{\partial \boldsymbol{n}} = 0, \quad \boldsymbol{u} = \boldsymbol{0}, \quad \text{on } \partial\Omega. \tag{3.16}$$

We construct k-th order fully decoupled and bound/positivity preserving R-GSAV schemes for the above system as follows.

Scheme 3.1 *(k-th order fully decoupled and bound/positivity preserving R-GSAV schemes).* Given $(v^j, \rho^j, c^j, \boldsymbol{u}^j, r^j, p^j)$, $j = n, n-1, \ldots, n-k+1$, we find $(v^{n+1}, \rho^{n+1}, c^{n+1}, \boldsymbol{u}^{n+1}, r^{n+1}, p^{n+1})$ as follows:

$$\begin{aligned}\frac{\alpha_k v^{n+1} - A_k(v^n)}{\delta t} - \Delta v^{n+1} &= -B_k(\boldsymbol{u}^n \cdot \nabla v^n) + |\nabla B_k(v^n)|^2 \\ &\quad - \frac{1}{\exp\left(B_k(v^n)\right)} \nabla \cdot \left(\eta(B_k(\rho^n)) \nabla B_k(c^n)\right),\end{aligned} \tag{3.17}$$

$$\left(\exp(B_k(v^n)) \frac{\partial v^{n+1}}{\partial \boldsymbol{n}} - \eta(B_k(\rho^n)) \frac{\partial B_k(c^n)}{\partial \boldsymbol{n}}\right)|_{\partial\Omega} = 0,$$

$$\bar{\rho}^{n+1} = \exp(v^{n+1}), \tag{3.18}$$

$$\lambda^{n+1} = \frac{\int_\Omega A_k(\rho^n) dx}{\int_\Omega \alpha_k \bar{\rho}^{n+1} dx}, \tag{3.19}$$

$$\rho^{n+1} = \lambda^{n+1} \bar{\rho}^{n+1}, \tag{3.20}$$

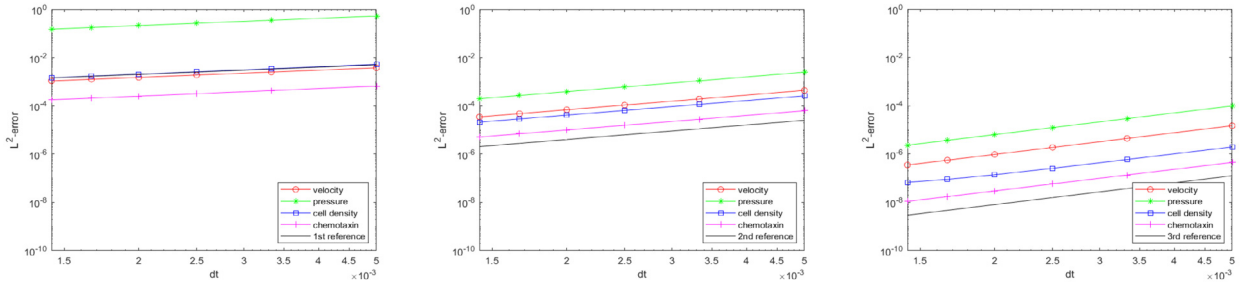

(a) first-order scheme (b) second-order scheme (c) third-order scheme

Fig. 1. Example 1: The convergence rates of positivity preserving Scheme 3.1 in the L^2-norm for the periodic PKS-NS system.

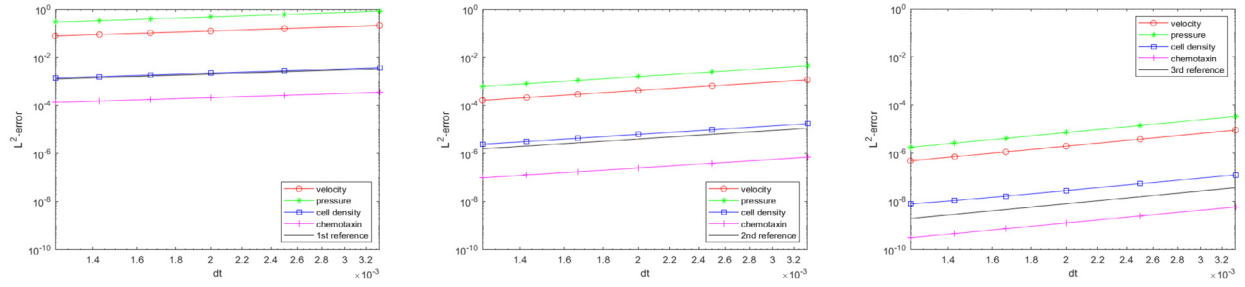

(a) first-order scheme (b) second-order scheme (c) third-order scheme

Fig. 2. Example 2: The convergence rates of bound preserving Scheme 3.1 in the L^2-norm for the non-periodic PKS-NS system.

$$-\Delta\overline{c}^{n+1}+\alpha\overline{c}^{n+1}=\rho^{n+1},\quad \frac{\partial\overline{c}^{n+1}}{\partial\boldsymbol{n}}|_{\partial\Omega}=0, \tag{3.21}$$

$$\frac{\alpha_k\overline{\boldsymbol{u}}^{n+1}-A_k(\overline{\boldsymbol{u}}^n)}{\delta t}-\nu\Delta\overline{\boldsymbol{u}}^{n+1}=-B_k(\overline{\boldsymbol{u}}^n\cdot\nabla\overline{\boldsymbol{u}}^n)-\nabla B_k(p^n)+\rho^{n+1}\nabla\overline{c}^{n+1}, \tag{3.22}$$

$$\overline{\boldsymbol{u}}^{n+1}|_{\partial\Omega}=0,$$

$$\frac{\widetilde{r}^{n+1}-r^n}{\delta t}=-\frac{\widetilde{r}^{n+1}}{E(\overline{\rho}^{n+1},\overline{c}^{n+1},\overline{\boldsymbol{u}}^{n+1})}G(\overline{\rho}^{n+1},\overline{c}^{n+1},\overline{\boldsymbol{u}}^{n+1}), \tag{3.23}$$

$$\xi^{n+1}=\frac{\widetilde{r}^{n+1}}{E(\overline{\rho}^{n+1},\overline{c}^{n+1},\overline{\boldsymbol{u}}^{n+1})},\quad \eta_k^{n+1}=1-\left(1-\xi^{n+1}\right)^k, \tag{3.24}$$

$$c^{n+1}=\eta_k^{n+1}\overline{c}^{n+1},\quad \boldsymbol{u}^{n+1}=\eta_k^{n+1}\overline{\boldsymbol{u}}^{n+1}, \tag{3.25}$$

$$r^{n+1}=\zeta_0^{n+1}\widetilde{r}^{n+1}+(1-\zeta_0^{n+1})E(\rho^{n+1},c^{n+1},\boldsymbol{u}^{n+1}), \tag{3.26}$$

and

$$(\nabla p^{n+1},\nabla q)=(-\nu\nabla\times\nabla\times\boldsymbol{u}^{n+1}-\boldsymbol{u}^{n+1}\cdot\nabla\boldsymbol{u}^{n+1}+\rho^{n+1}\nabla c^{n+1},\nabla q),\quad \forall q\in H^1(\Omega), \tag{3.27}$$

where $\zeta_0^{n+1}\in[0,1]$ is a parameter to be determined in the admissible set

$$\mathcal{V}=\left\{\zeta\in[0,1]s.t.\frac{r^{n+1}-\widetilde{r}^{n+1}}{\delta t}=-\gamma^{n+1}G(\rho^{n+1},c^{n+1},\boldsymbol{u}^{n+1})+\frac{\widetilde{r}^{n+1}G(\overline{\rho}^{n+1},\overline{c}^{n+1}\overline{\boldsymbol{u}}^{n+1})}{E(\overline{\rho}^{n+1},\overline{c}^{n+1},\overline{\boldsymbol{u}}^{n+1})}\right\}, \tag{3.28}$$

with $\gamma^{n+1}\geq 0$ to be determined so that $\mathcal{V}$ is not empty. In the above α_k, A_k and $B_k\,(k=1,2,3)$ are given by:
first-order scheme:

$$\alpha_1=1,\quad A_1\left(v^n\right)=v^n,\quad B_1\left(w^n\right)=w^n;$$

second-order scheme:

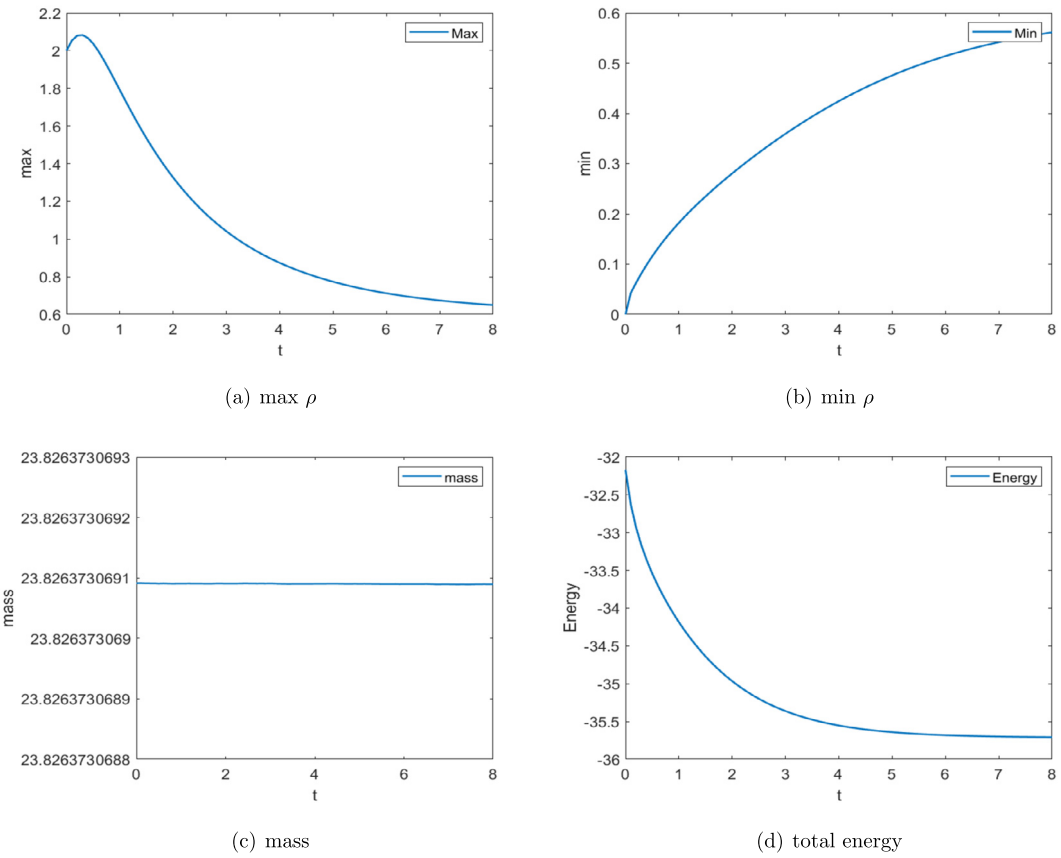

(a) max ρ (b) min ρ

(c) mass (d) total energy

Fig. 3. Example 3: Evolutions of max ρ, min ρ, mass of ρ, and total energy E_{tot} with initial data (4.3).

$$\alpha_2 = \frac{3}{2}, \quad A_2\left(v^n\right) = 2v^n - \frac{1}{2}v^{n-1}, \quad B_2\left(w^n\right) = 2w^n - w^{n-1};$$

third-order scheme:

$$\alpha_3 = \frac{11}{6}, \quad A_3\left(v^n\right) = 3v^n - \frac{3}{2}v^{n-1} + \frac{1}{3}v^{n-2}, \quad B_3\left(w^n\right) = 3w^n - 3w^{n-1} + w^{n-2}.$$

The formulae for $k = 4, 5, 6$ can be derived similarly.

Remark 3.1. We emphasize that Scheme 3.1 is totally decoupled, and can be solved consecutively. In fact, the main computational costs are (i) Solving v^{n+1} from (3.17); (ii) Solving $\overline{\boldsymbol{u}}^{n+1}$ from (3.22); and (iii) Solving p^{n+1} from (3.27). Note that these are all elliptic equations with constant coefficients so they can be solved very efficiently.

We now discuss how to determine ζ_0^{n+1} and γ^{n+1}. Plugging the equation (3.26) into (3.28), we observe that if we choose ζ_0^{n+1} and γ^{n+1} such that

$$\begin{aligned}\left(\tilde{r}^{n+1} - E(\rho^{n+1}, c^{n+1}, \boldsymbol{u}^{n+1})\right)\zeta_0^{n+1} =& \tilde{r}^{n+1} - E(\rho^{n+1}, c^{n+1}, \boldsymbol{u}^{n+1}) - \delta t\gamma^{n+1}G(\rho^{n+1}, c^{n+1}, \boldsymbol{u}^{n+1}) \\ &+ \delta t\frac{\tilde{r}^{n+1}G(\overline{\rho}^{n+1}, \overline{c}^{n+1}, \overline{\boldsymbol{u}}^{n+1})}{E(\overline{\rho}^{n+1}, \overline{c}^{n+1}, \overline{\boldsymbol{u}}^{n+1})},\end{aligned} \tag{3.29}$$

then, $\zeta_0^{n+1} \in \mathcal{V}$.

The choice of ζ_0^{n+1} and γ^{n+1} as well as properties of Scheme 3.1 are summarized in the theorem below.

Theorem 3.1. *We choose ζ_0^{n+1} in (3.26) and γ^{n+1} in (3.28) as follows:*

1. *If $\tilde{r}^{n+1} = E(\rho^{n+1}, c^{n+1}, \boldsymbol{u}^{n+1})$, we set $\zeta_0^{n+1} = 0$ and $\gamma^{n+1} = \frac{\tilde{r}^{n+1}G(\overline{\rho}^{n+1}, \overline{c}^{n+1}, \overline{\boldsymbol{u}}^{n+1})}{E(\overline{\rho}^{n+1}, \overline{c}^{n+1}, \overline{\boldsymbol{u}}^{n+1})G(\rho^{n+1}, c^{n+1}, \boldsymbol{u}^{n+1})}$.*

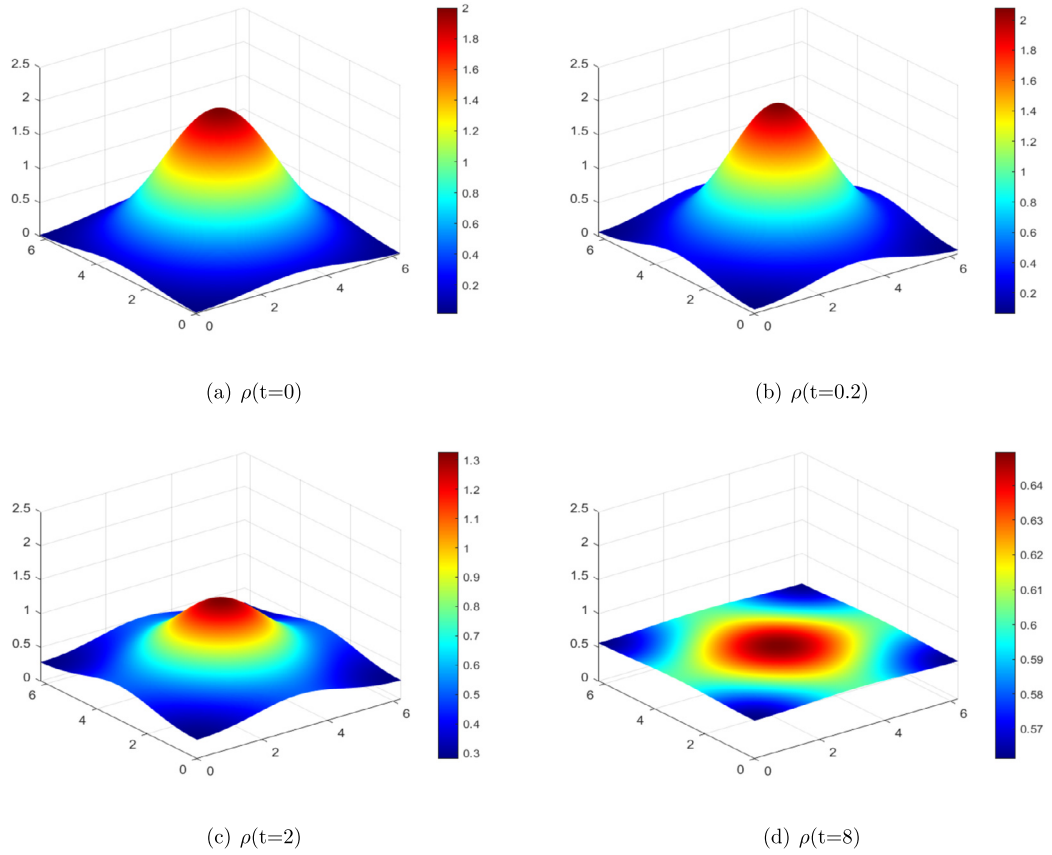

(a) ρ(t=0) (b) ρ(t=0.2)

(c) ρ(t=2) (d) ρ(t=8)

Fig. 4. Example 3: Snapshots of the cell density ρ for the chemotactic non-aggregation. (For interpretation of the colors in the figure(s), the reader is referred to the web version of this article.)

2. *If* $\widetilde{r}^{n+1} > E(\rho^{n+1}, c^{n+1}, \boldsymbol{u}^{n+1})$, *we set* $\zeta_0^{n+1} = 0$ *and* $\gamma^{n+1} = \frac{\widetilde{r}^{n+1} - E(\rho^{n+1}, c^{n+1}, \boldsymbol{u}^{n+1})}{\delta t G(\rho^{n+1}, c^{n+1}, \boldsymbol{u}^{n+1})} + \frac{\widetilde{r}^{n+1} G(\overline{\rho}^{n+1}, \overline{c}^{n+1}, \overline{\boldsymbol{u}}^{n+1})}{E(\overline{\rho}^{n+1}, \overline{c}^{n+1}, \overline{\boldsymbol{u}}^{n+1}) G(\rho^{n+1}, c^{n+1}, \boldsymbol{u}^{n+1})}$.
3. *If* $\widetilde{r}^{n+1} < E(\rho^{n+1}, c^{n+1}, \boldsymbol{u}^{n+1})$ *and* $\widetilde{r}^{n+1} - E(\rho^{n+1}, c^{n+1}, \boldsymbol{u}^{n+1}) + \delta t \frac{\widetilde{r}^{n+1} G(\overline{\rho}^{n+1}, \overline{c}^{n+1}, \overline{\boldsymbol{u}}^{n+1})}{E(\overline{\rho}^{n+1}, \overline{c}^{n+1}, \overline{\boldsymbol{u}}^{n+1})} \geq 0$, *we set* $\zeta_0^{n+1} = 0$ *and* $\gamma^{n+1} = \frac{\widetilde{r}^{n+1} - E(\rho^{n+1}, c^{n+1}, \boldsymbol{u}^{n+1})}{\delta t G(\rho^{n+1}, c^{n+1}, \boldsymbol{u}^{n+1})} + \frac{\widetilde{r}^{n+1} G(\overline{\rho}^{n+1}, \overline{c}^{n+1}, \overline{\boldsymbol{u}}^{n+1})}{E(\overline{\rho}^{n+1}, \overline{c}^{n+1}, \overline{\boldsymbol{u}}^{n+1}) G(\rho^{n+1}, c^{n+1}, \boldsymbol{u}^{n+1})}$.
4. *If* $\widetilde{r}^{n+1} < E(\rho^{n+1}, c^{n+1}, \boldsymbol{u}^{n+1})$ *and* $\widetilde{r}^{n+1} - E(\rho^{n+1}, c^{n+1}, \boldsymbol{u}^{n+1}) + \delta t \frac{\widetilde{r}^{n+1} G(\overline{\rho}^{n+1}, \overline{c}^{n+1}, \overline{\boldsymbol{u}}^{n+1})}{E(\overline{\rho}^{n+1}, \overline{c}^{n+1}, \overline{\boldsymbol{u}}^{n+1})} < 0$, *we set* $\zeta_0^{n+1} = 1 - \frac{\delta t \widetilde{r}^{n+1} G(\overline{\rho}^{n+1}, \overline{c}^{n+1}, \overline{\boldsymbol{u}}^{n+1})}{E(\overline{\rho}^{n+1}, \overline{c}^{n+1}, \overline{\boldsymbol{u}}^{n+1})(E(\rho^{n+1}, c^{n+1}, \boldsymbol{u}^{n+1}) - \widetilde{r}^{n+1})}$ *and* $\gamma^{n+1} = 0$.

Then, (3.29) is satisfied in all cases above and $\zeta_0^{n+1} \in \mathcal{V}$. *Besides, given* $\rho^j > 0$ *such that*

$$\int_\Omega \rho^j dx = \int_\Omega \rho^0 dx, \quad j = n, n-1, \ldots, n-k+1. \tag{3.30}$$

The Scheme 3.1 is uniquely solvable and satisfies the following properties unconditionally:

- *Positivity preserving:* $\rho^{n+1} > 0$.
- *Mass conserving:* $\int_\Omega \rho^{n+1} dx = \int_\Omega \rho^0 dx$.
- *Given* $r^n \geq 0$, *we have* $r^{n+1} \geq 0$, $\xi^{n+1} \geq 0$, *and the Scheme 3.1 is unconditionally stable in the sense that the modified energy satisfies*

$$r^{n+1} - r^n = -\delta t \gamma^{n+1} G(\rho^{n+1}, c^{n+1}, \boldsymbol{u}^{n+1}) \leq 0. \tag{3.31}$$

Moreover,

$$r^{n+1} \leq E(\rho^{n+1}, c^{n+1}, \boldsymbol{u}^{n+1}), \quad \forall n. \tag{3.32}$$

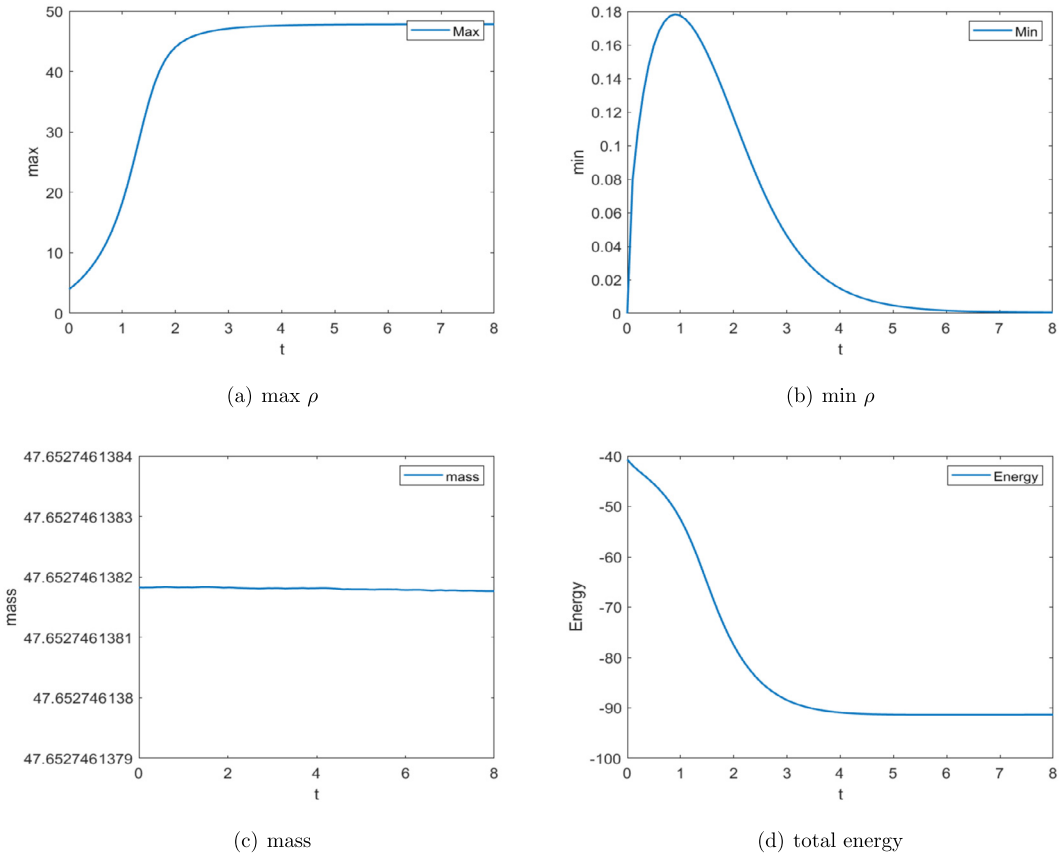

(a) max ρ (b) min ρ

(c) mass (d) total energy

Fig. 5. Example 4: Evolutions of max ρ, min ρ, mass of ρ, and total energy E_{tot} with initial data (4.4).

- *There exists a constant $M_k > 0$ such that*

$$\int_\Omega \left(\frac{1}{2}|\nabla c^n|^2 + \frac{\alpha}{4}(c^n)^2\right) dx \le M_k^2, \quad \forall n. \tag{3.33}$$

Proof. From (3.18), we have $\bar{\rho}^{n+1} > 0$.

Based on (3.30) and the definition of coefficients α_k and A_k, we have

$$\int_\Omega A_k(\rho^n) dx = \alpha_k \int_\Omega \rho^0 dx. \tag{3.34}$$

Followed by (3.34) and (3.19), we obtain

$$\lambda^{n+1} \int_\Omega \bar{\rho}^{n+1} dx = \int_\Omega \rho^0 dx. \tag{3.35}$$

Thanks to $\bar{\rho}^{n+1} > 0$, we know that $\lambda^{n+1} > 0$. Then (3.20) implies $\rho^{n+1} > 0$. Therefore, we derive that $\int_\Omega \rho^{n+1} dx = \int_\Omega \rho^0 dx$.

Given $r^n \ge 0$, it follows from (3.23) that

$$\tilde{r}^{n+1} = \frac{r^n}{1 + \delta t \frac{G(\overline{\rho}^{n+1}, \overline{c}^{n+1}, \overline{\boldsymbol{u}}^{n+1})}{E(\overline{\rho}^{n+1}, \overline{c}^{n+1}, \overline{\boldsymbol{u}}^{n+1})}} \ge 0 \tag{3.36}$$

since that $G(\overline{\rho}^{n+1}, \overline{c}^{n+1}, \overline{\boldsymbol{u}}^{n+1}) \ge 0$ and $E(\overline{\rho}^{n+1}, \overline{c}^{n+1}, \overline{\boldsymbol{u}}^{n+1}) > 0$. Then (3.24) implies $\xi^{n+1} \ge 0$ and (3.26) implies $r^{n+1} \ge 0$. Additionally, we get (3.31) by combining (3.23) and (3.28).

In Cases 1-3, we have $\zeta_0^{n+1} = 0$ so $r^{n+1} = E(\rho^{n+1}, c^{n+1}, \boldsymbol{u}^{n+1})$. In Case 4, due to $\zeta_0^{n+1} = 1 - \frac{\delta t \tilde{r}^{n+1} G(\overline{\rho}^{n+1}, \overline{c}^{n+1}, \overline{\boldsymbol{u}}^{n+1})}{E(\overline{\rho}^{n+1}, \overline{c}^{n+1}, \overline{\boldsymbol{u}}^{n+1})(E(\rho^{n+1}, c^{n+1}, \boldsymbol{u}^{n+1}) - \tilde{r}^{n+1})} \in [0, 1]$ and $\tilde{r}^{n+1} < E(\rho^{n+1}, c^{n+1}, \boldsymbol{u}^{n+1})$, we know that $r^{n+1} \le E(\rho^{n+1}, c^{n+1}, \boldsymbol{u}^{n+1})$ from (3.26).

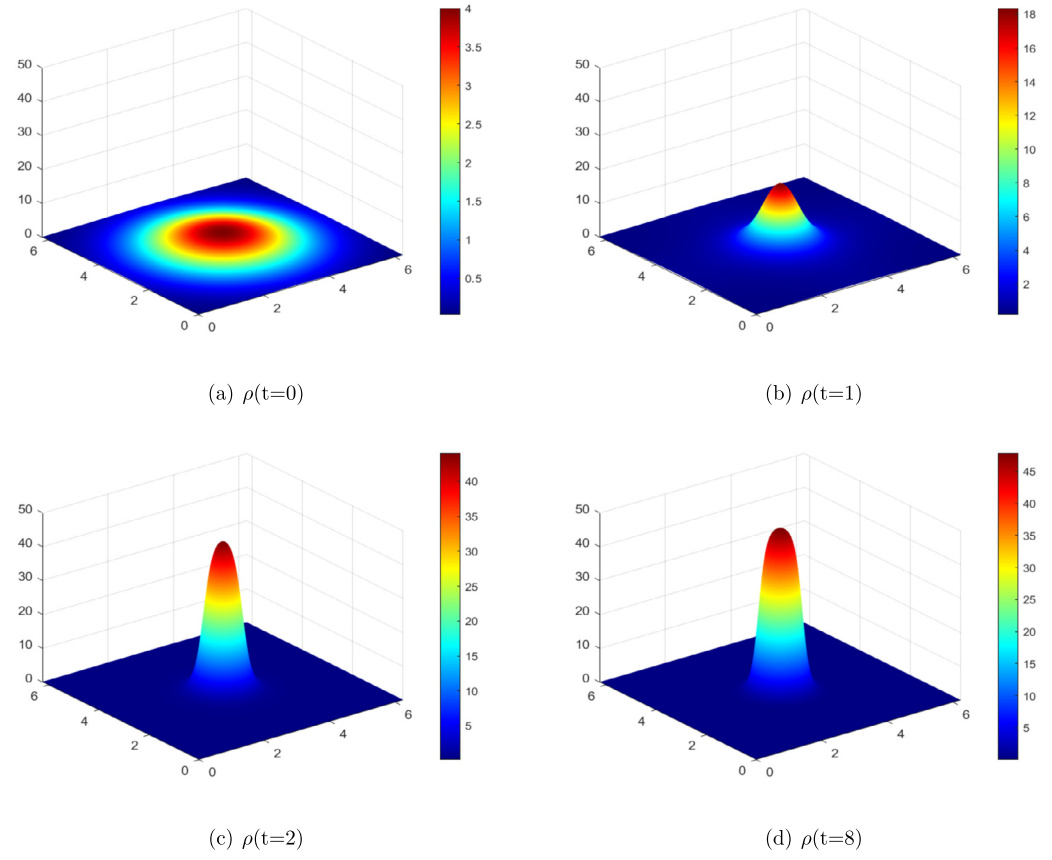

(a) ρ(t=0) (b) ρ(t=1)

(c) ρ(t=2) (d) ρ(t=8)

Fig. 6. Example 4: Snapshots of the cell density ρ for the chemotactic aggregation with a saturation concentration.

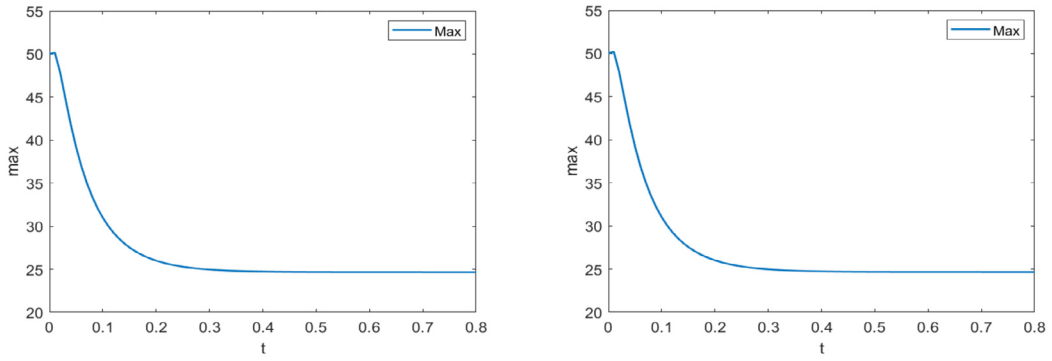

(a) max ρ of PKS system (b) max ρ of PKS-NS system

Fig. 7. Example 5: Evolutions of max ρ of the PKS system and PKS-NS system with initial data (4.5).

We denote $M_0 := r^0 = E(\rho(\cdot,0), c(\cdot,0), \boldsymbol{u}(\cdot,0))$ and have $\widetilde{r}^{n+1} \le M_0$ $(\forall n)$ from (3.31) and (3.36). Setting

$$E_{tot}(\rho^n, c^n, \boldsymbol{u}^n) = \int_\Omega \left(f(\rho^n) - \rho^n c^n + \frac{\alpha}{4}(c^n)^2 + \frac{1}{2}|\boldsymbol{u}^n|^2 \right) dx + \int_\Omega \left(\frac{1}{2}|\nabla c^n|^2 + \frac{\alpha}{4}(c^n)^2 \right) dx$$
$$:= E_1(\rho^n, c^n, \boldsymbol{u}^n) + E_0(c^n),$$

since $f(\rho^n) = \rho^n \log(\rho^n) - \rho^n$ is strictly convex and $E_1(\rho^n, c^n, \boldsymbol{u}^n)$ is bounded from below, there exists $C_0 > 0$ such that $E_1(\rho^n, c^n, \boldsymbol{u}^n) + C_0 > 1$ for all ρ^n and c^n. Then we derive from (3.24) that

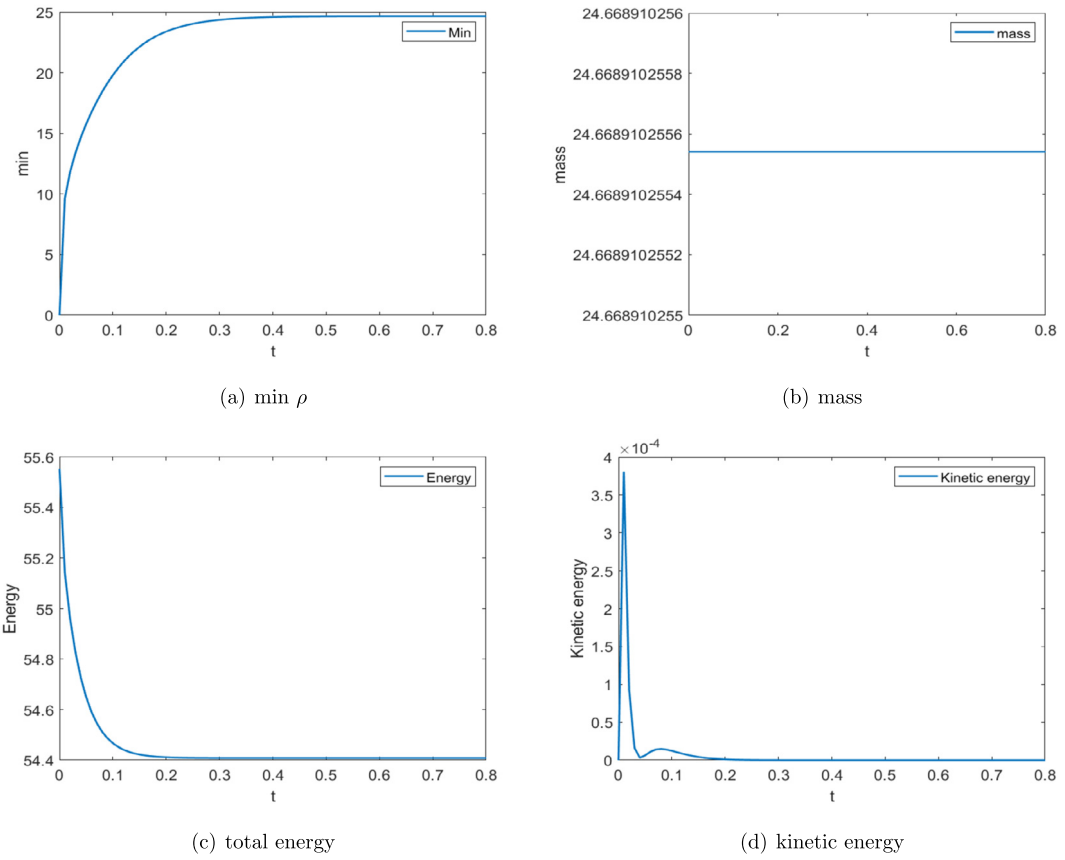

(a) min ρ (b) mass

(c) total energy (d) kinetic energy

Fig. 8. Example 5: Evolutions of min ρ, mass of ρ, total energy E_{tot}, and kinetic energy of the PKS-NS system with initial data (4.5).

$$| \xi^{n+1} | = \frac{\widetilde{r}^{n+1}}{E(\overline{\rho}^{n+1}, \overline{c}^{n+1}, \overline{\boldsymbol{u}}^{n+1})} \leq \frac{M_0}{E_0(\overline{c}^{n+1}) + 1}. \tag{3.37}$$

For $\eta_k^{n+1} = 1 - \left(1 - \xi^{n+1}\right)^k$, there exists a polynomial P_{k-1} of $k-1$ and a constant $M_k > 0$ such that

$$| \eta_k^{n+1} | = | \xi^{n+1} P_{k-1}(\xi^{n+1}) | \leq \frac{M_k}{E_0(\overline{c}^{n+1}) + 1}. \tag{3.38}$$

Indeed, $\sqrt{A} \leq A + 1$ for all $A \geq 0$. Therefore, we derive from (3.25) that

$$\sqrt{E_0(c^{n+1})} = | \eta_k^{n+1} | \sqrt{E_0(\overline{c}^{n+1})} \leq M_k.$$

That is,

$$\int_\Omega \left(\frac{1}{2} |\nabla c^n|^2 + \frac{\alpha}{4} (c^n)^2 \right) dx \leq M_k^2, \quad \forall n,$$

which completes the proof. □

Remark 3.2. Note that in most cases, we can choose $\zeta_0^{n+1} = 0$ which implies that $r^{n+1} = E(\rho^{n+1}, c^{n+1}, \boldsymbol{u}^{n+1})$. Then, we can derive from (3.31) and (3.32) that

$$E(\rho^{n+1}, c^{n+1}, \boldsymbol{u}^{n+1}) = r^{n+1} \leq r^n \leq E(\rho^n, c^n, \boldsymbol{u}^n),$$

i.e., the original energy is also dissipative when $\zeta_0^{n+1} = 0$.

We note that the above result carries over to fully discretized versions of Scheme 3.1 using Galerkin-type spatial discretizations with consistent discrete integration by parts.

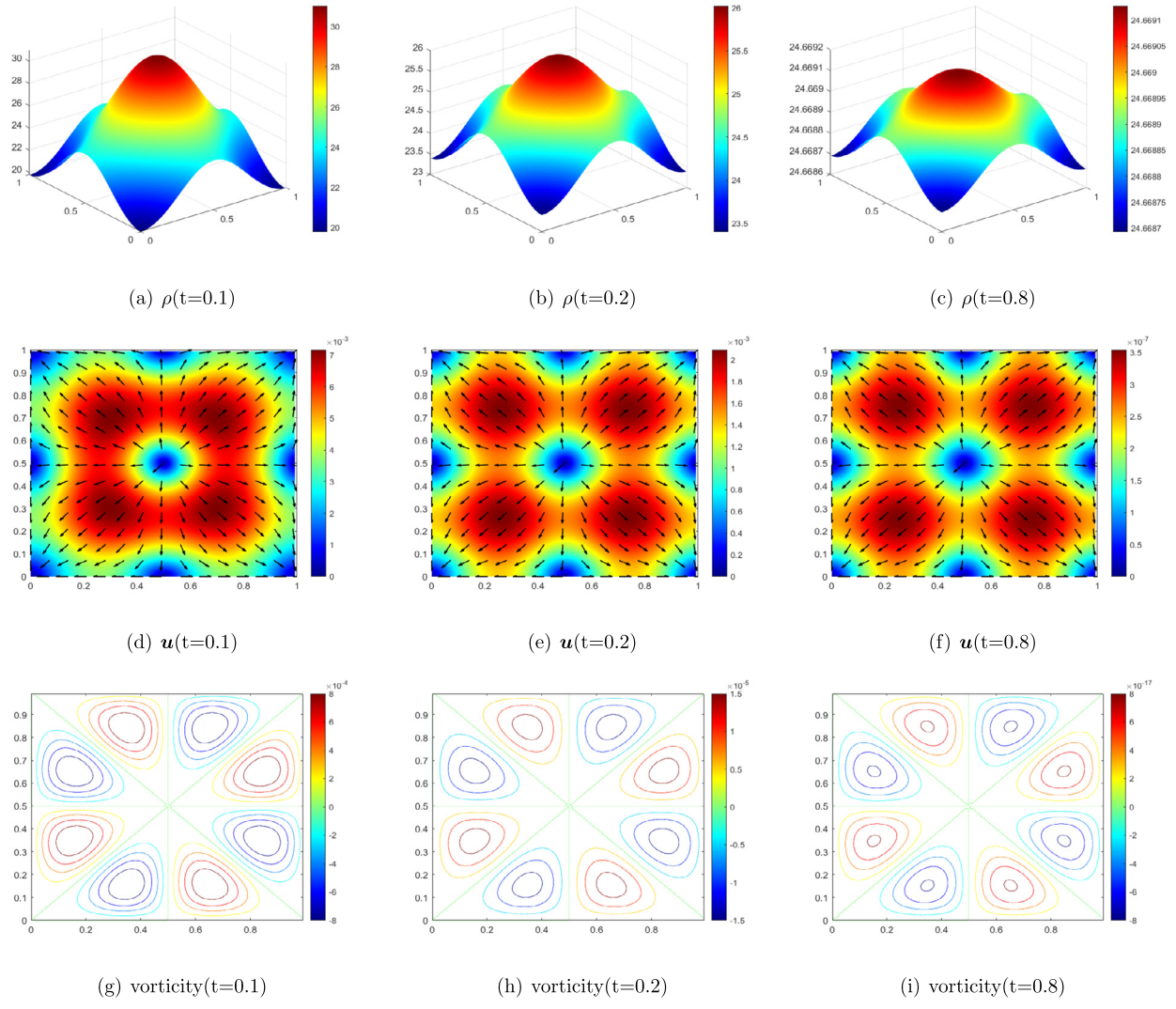

(a) ρ(t=0.1) (b) ρ(t=0.2) (c) ρ(t=0.8)

(d) $\boldsymbol{u}$(t=0.1) (e) $\boldsymbol{u}$(t=0.2) (f) $\boldsymbol{u}$(t=0.8)

(g) vorticity(t=0.1) (h) vorticity(t=0.2) (i) vorticity(t=0.8)

Fig. 9. Example 5: Snapshots of the cell density ρ, fluid velocity **u**, and vorticity contours of the PKS-NS system with initial data (4.5).

4. Numerical experiments

In this section, we first carry out some numerical experiments to confirm the accuracy of our fully decoupled R-GSAV schemes for the PKS-NS system (2.1)-(2.5). Then, we provide two numerical examples to simulate the chemotactic non-aggregation and aggregation with a saturation concentration, as well as to validate the properties of bound preserving, energy dissipation and mass conservation. Finally, we present a series of numerical examples to investigate chemotactic blow-up of the PKS-NS system, and to validate the property of positivity preserving.

In all computations below, we use Fourier spectral method [3] in the directions with periodic boundary conditions, and the Legendre-Galerkin method [38] in the directions with non-periodic boundary conditions.

4.1. Accuracy test

We start by checking the accuracy of Scheme 3.1 ($k = 1, 2, 3$) for the PKS-NS system subject to different coefficients and boundary conditions.

Example 1. *The PKS-NS system with $\eta(\rho) = \rho$, $\alpha = 0$ and $\nu = 1$ in $\Omega = (0, 2) \times (0, 2)$ with periodic boundary conditions.* We set exact solutions as follows

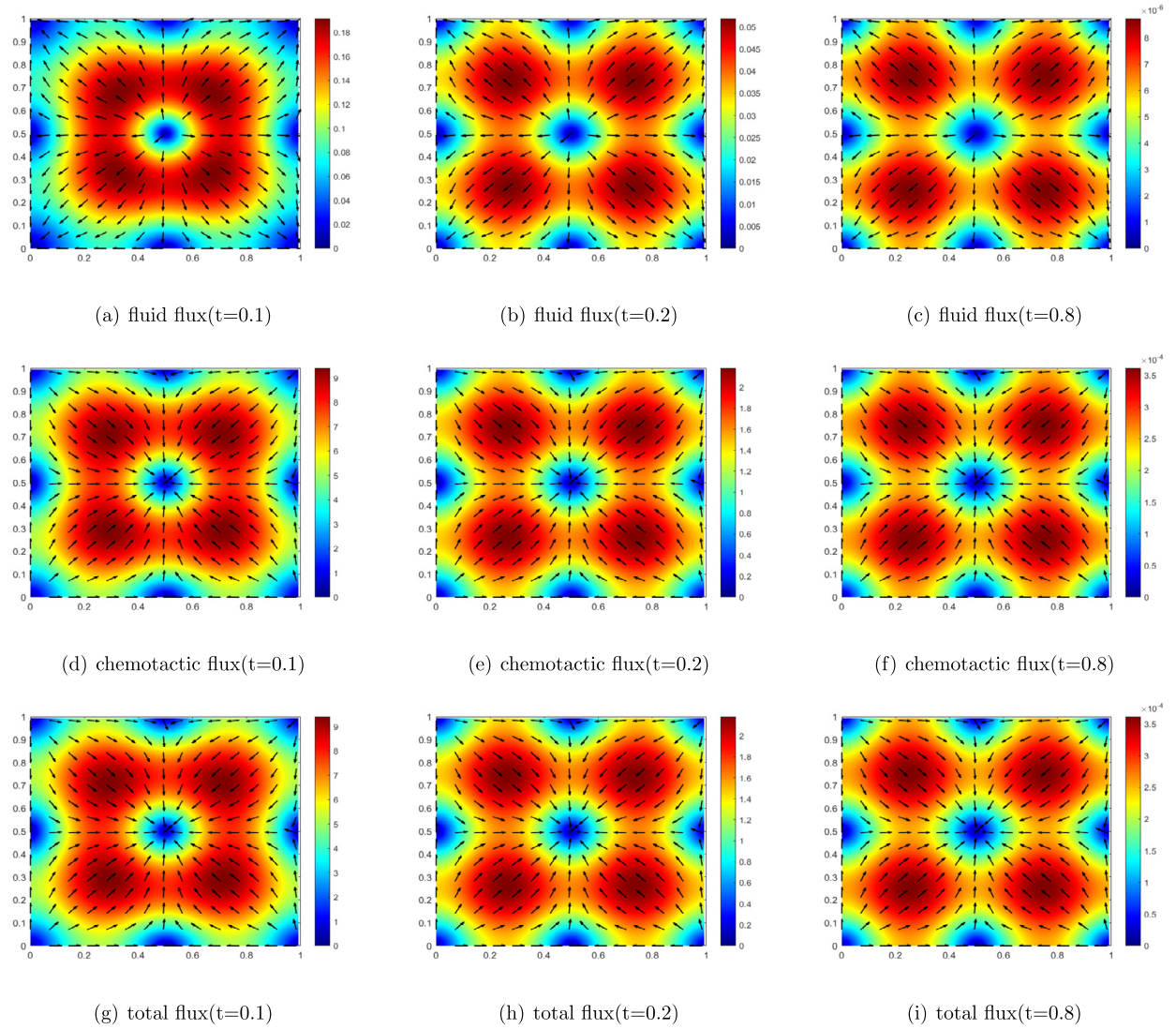

(a) fluid flux(t=0.1) (b) fluid flux(t=0.2) (c) fluid flux(t=0.8)

(d) chemotactic flux(t=0.1) (e) chemotactic flux(t=0.2) (f) chemotactic flux(t=0.8)

(g) total flux(t=0.1) (h) total flux(t=0.2) (i) total flux(t=0.8)

Fig. 10. Example 5: Vector plots of the fluid flux $\rho\mathbf{u}$, chemotactic flux $-\nabla\rho + \rho\nabla c$ and total flux $\rho\mathbf{u} - \nabla\rho + \rho\nabla c$ of the PKS-NS system with initial data (4.5).

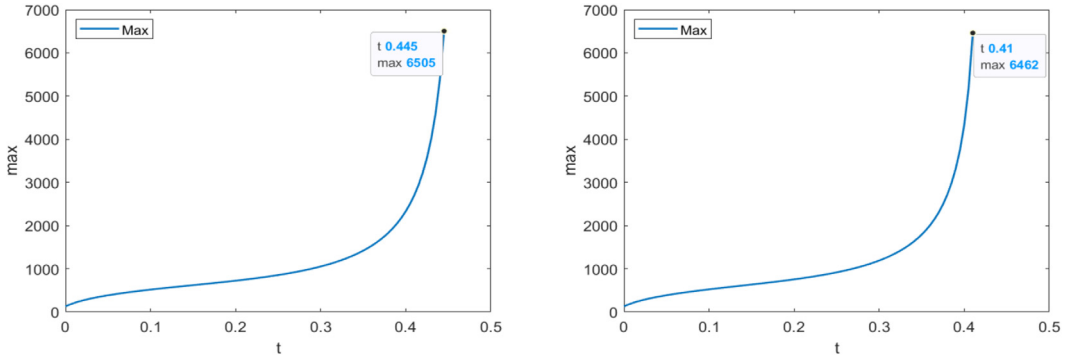

(a) max ρ of PKS system (b) max ρ of PKS-NS system

Fig. 11. Example 6: Evolutions of max ρ of the PKS system and PKS-NS system with initial data (4.6).

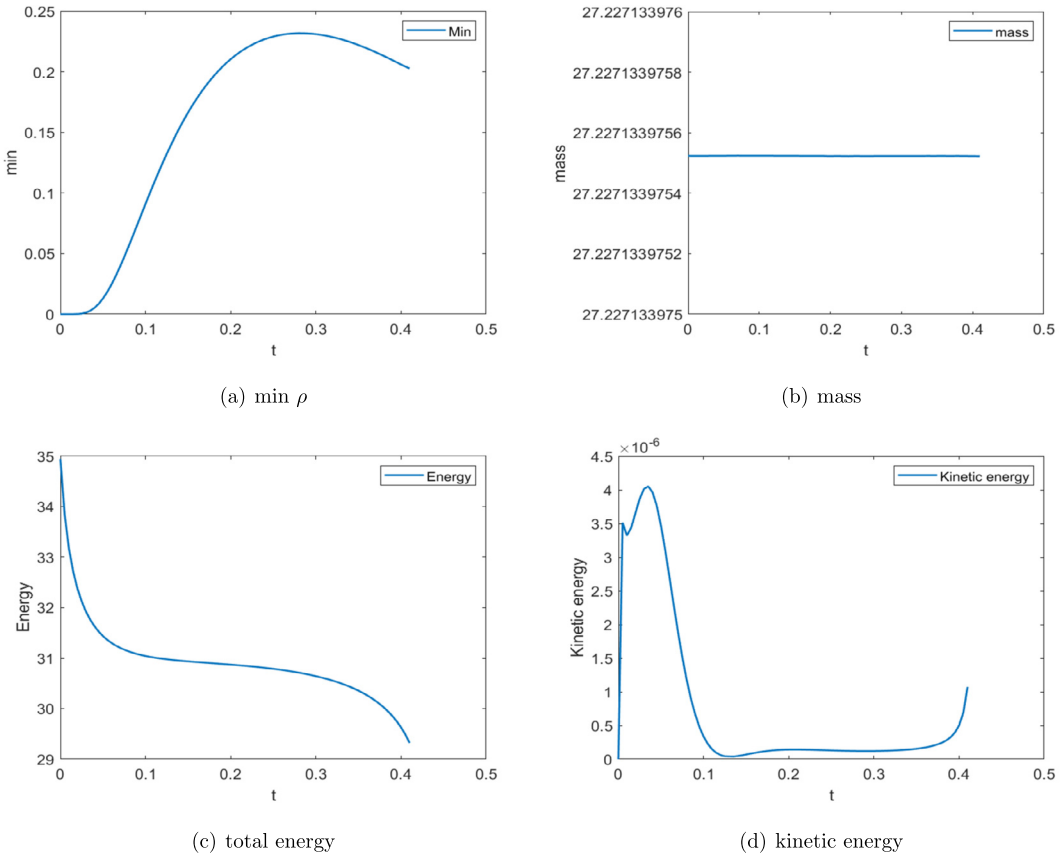

(a) min ρ (b) mass

(c) total energy (d) kinetic energy

Fig. 12. Example 6: Evolutions of min ρ, mass of ρ, total energy E_{tot}, and kinetic energy of the PKS-NS system with initial data (4.6).

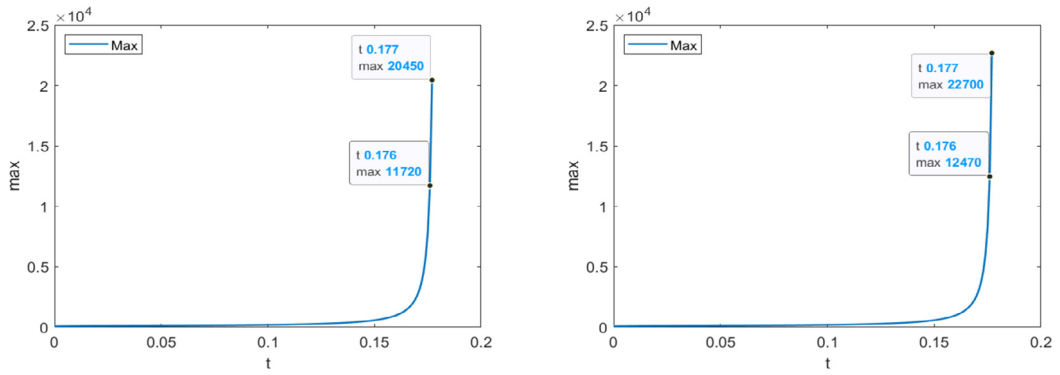

(a) max ρ of PKS system (b) max ρ of PKS-NS system

Fig. 13. Example 7: Evolutions of max ρ of the PKS system and PKS-NS system with initial data (4.7).

$$\begin{cases} u_1 = \pi \exp(\sin(\pi x)) \exp(\sin(\pi y)) \cos(\pi y) \sin^2(t), \\ u_2 = -\pi \exp(\sin(\pi x)) \exp(\sin(\pi y)) \cos(\pi x) \sin^2(t), \\ p = \exp(\cos(\pi x) \sin(\pi y)) \sin^2(t), \\ \rho = c = \sin(\pi x) \sin(\pi y) \sin(t) + 1.1. \end{cases} \tag{4.1}$$

We apply Fourier-spectral method in space with 32×32 modes so that the spatial discretization error is negligible with respect to the time discretization error. The convergence rates in the L^2-norm for the PKS-NS system at $T = 1$ by using first- to third-order schemes are shown in Fig. 1, which are consistent with orders of these schemes.

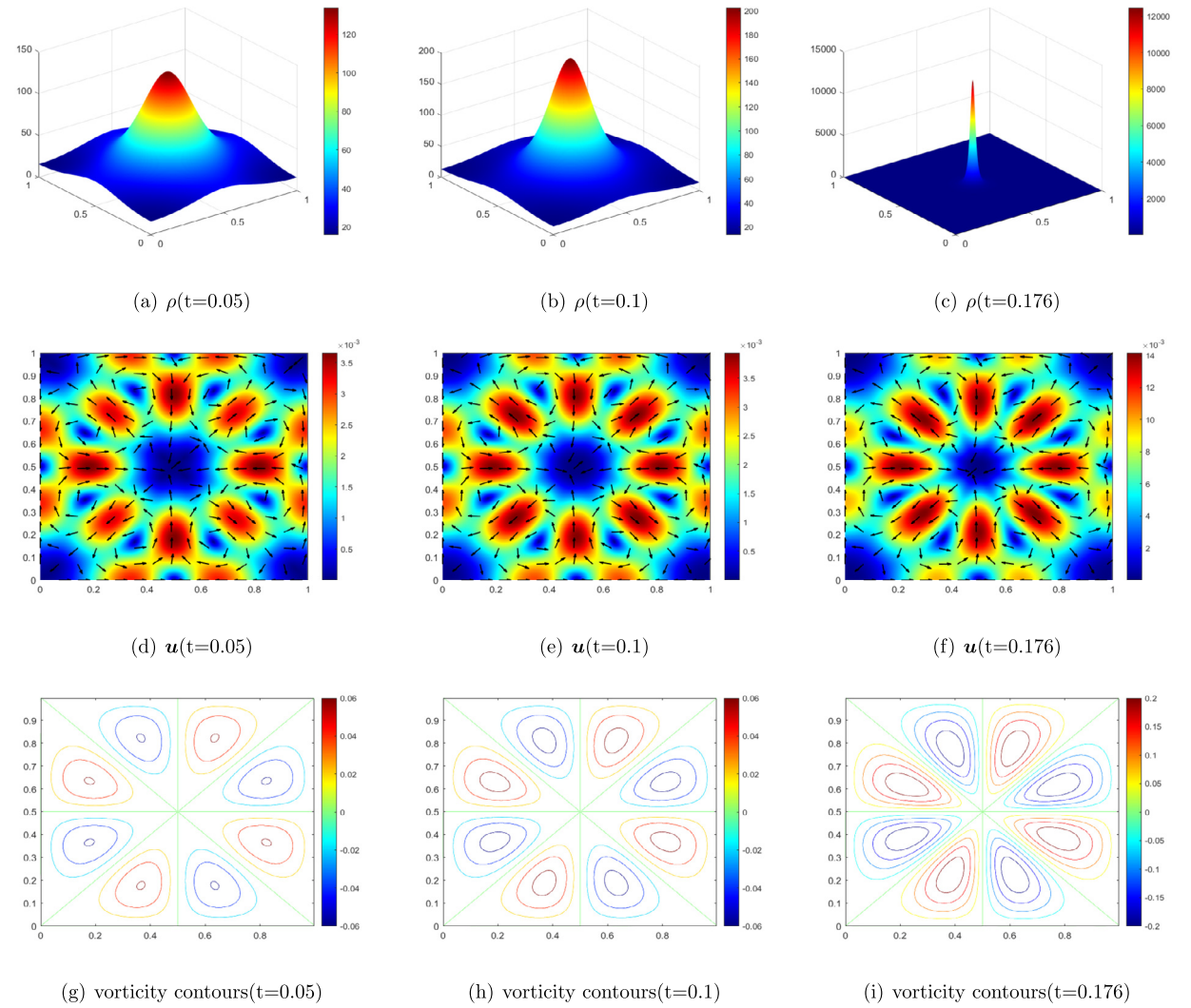

(a) ρ(t=0.05) (b) ρ(t=0.1) (c) ρ(t=0.176)

(d) $\boldsymbol{u}$(t=0.05) (e) $\boldsymbol{u}$(t=0.1) (f) $\boldsymbol{u}$(t=0.176)

(g) vorticity contours(t=0.05) (h) vorticity contours(t=0.1) (i) vorticity contours(t=0.176)

Fig. 14. Example 7: Snapshots of the cell density ρ, fluid velocity $\mathbf{u}$, and vorticity contours of the PKS-NS system with initial data (4.7).

Example 2. *The PKS-NS system with* $\eta(\rho) = \rho(1 - \frac{\rho}{M})$, $M = 3$, $\alpha = 1$ *and* $\nu = 0.01$ *in* $\Omega = (-1, 1) \times (-1, 1)$ *with non-periodic boundary conditions (2.6).* We change exact solutions as

$$\begin{cases} u_1 = \pi \sin(\pi x)^2 \sin(2\pi y) \sin(t), \\ u_2 = -\pi \sin(2\pi x) \sin(\pi y)^2 \sin(t), \\ p = \cos(\pi x) \sin(\pi y) \sin(t), \\ \rho = c = \cos(\pi x) \cos(\pi y) \sin(t) + 1.1. \end{cases} \tag{4.2}$$

We use the Legendre Galerkin method in space with 60×60 modes. The convergence rates with $k = 1, 2, 3$ in the L^2-norm for the PKS-NS system at $T = 1$ are plotted in Fig. 2. We observe that all the convergence rates are consistent with the order of the corresponding scheme.

4.2. Simulations of the chemotactic non-aggregation and aggregation

To validate the property of bound preserving for the cell density, we fix $\eta(\rho) = \rho(1 - \frac{\rho}{M})$ with a saturation concentration $M = 50$ for the PKS-NS system (2.1)-(2.5) in a bounded domain $\Omega = (0, 2\pi) \times (0, 2\pi)$ with periodic boundary conditions. Besides, the initial fluid velocity $\mathbf{u}_0 = \mathbf{0}$, the viscosity coefficient $\nu = 1$ and the consumption rate $\alpha = 0$ unless otherwise specified. We use the Fourier-spectral method in space with 128×128 modes, and first order Scheme 3.1 ($k = 1$) with time step $\delta t = 10^{-3}$ for simulations in this subsection.

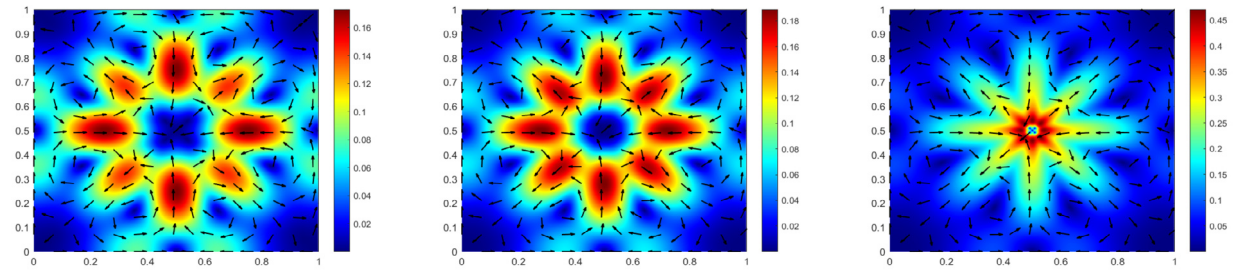

(a) fluid flux(t=0.05) (b) fluid flux(t=0.1) (c) fluid flux(t=0.176)

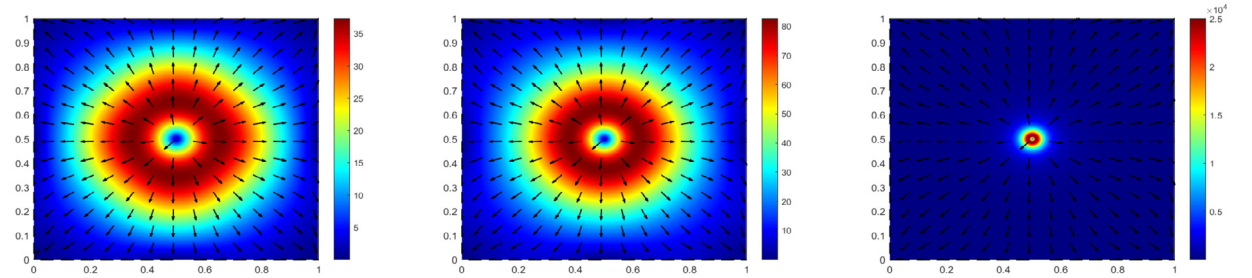

(d) chemotactic flux(t=0.05) (e) chemotactic flux(t=0.1) (f) chemotactic flux(t=0.176)

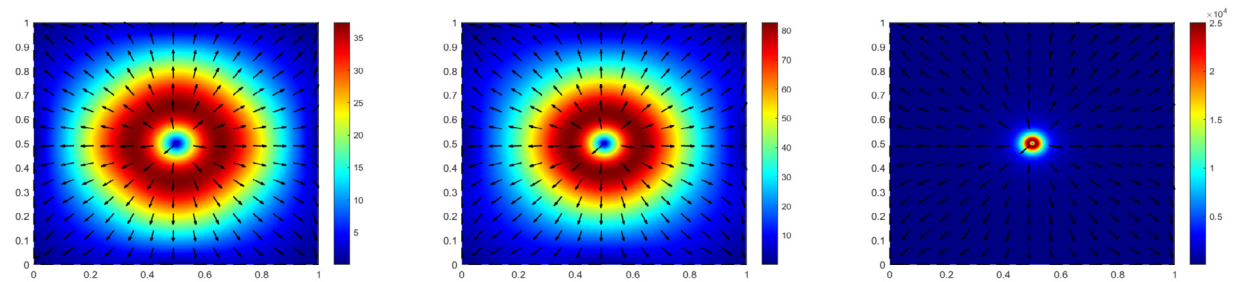

(g) total flux(t=0.05) (h) total flux(t=0.1) (i) total flux(t=0.176)

Fig. 15. Example 7: Vector plots of the fluid flux $\rho\mathbf{u}$, chemotactic flux $-\nabla\rho+\rho\nabla c$ and total flux $\rho\mathbf{u}-\nabla\rho+\rho\nabla c$ of the PKS-NS system with initial data (4.7).

Example 3. *Chemotactic non-aggregation.* Initial conditions are given by

$$\rho(x,y,0)=2\exp\big(-\frac{1}{4}\big((x-\pi)^2+(y-\pi)^2\big)\big). \tag{4.3}$$

The simulation is carried out until the system reaches the steady state at $t=8$. Fig. 3 displays evolutions of max ρ, min ρ, mass of ρ, and total energy E_{tot}. We observe that ρ remains in the interval $(0,M)$, the total energy is dissipative, and the mass of ρ is preserved at all time. Several snapshots of the cell density ρ are shown in Fig. 4. We observe that in this case there is no chemotactic accumulation for cells.

Example 4. *Chemotactic aggregation with a saturation concentration.* We change the initial conditions to

$$\rho(x,y,0)=4\exp\big(-\frac{1}{4}\big((x-\pi)^2+(y-\pi)^2\big)\big), \tag{4.4}$$

with a larger total mass of the cell density so that chemotactic accumulations could occur. Evolutions of max ρ, min ρ, mass of ρ and total energy E_{tot} are presented in Fig. 5. We observe that ρ still remains in the range of $(0,M)$, the total energy is dissipative, and the mass of ρ is conserved. Snapshots of the cells density are shown in Fig. 6 which indicates that the cells accumulate until the density reaches the largest concentration $M=50$.

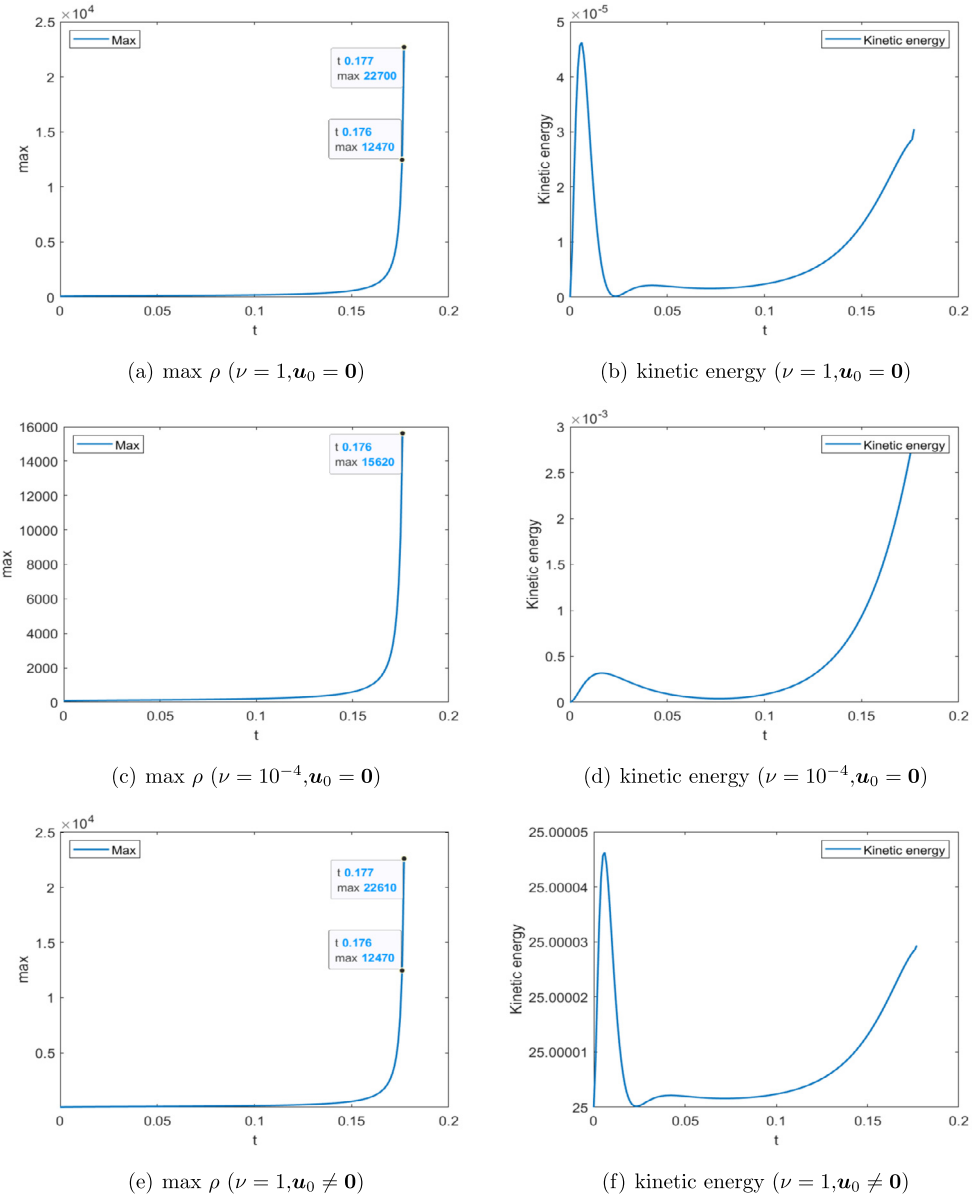

(a) max ρ ($\nu = 1, \boldsymbol{u}_0 = \mathbf{0}$) (b) kinetic energy ($\nu = 1, \boldsymbol{u}_0 = \mathbf{0}$)

(c) max ρ ($\nu = 10^{-4}, \boldsymbol{u}_0 = \mathbf{0}$) (d) kinetic energy ($\nu = 10^{-4}, \boldsymbol{u}_0 = \mathbf{0}$)

(e) max ρ ($\nu = 1, \boldsymbol{u}_0 \neq \mathbf{0}$) (f) kinetic energy ($\nu = 1, \boldsymbol{u}_0 \neq \mathbf{0}$)

Fig. 16. Example 8: Evolutions of max ρ and kinetic energy of the PKS-NS system with different ν and $\boldsymbol{u}_0$.

4.3. Investigation of the blow-up phenomenon

We consider the PKS-NS system (2.1)-(2.6) with $\eta(\rho) = \rho$, the viscosity coefficient is $\nu = 1$ unless otherwise specified.

We start with the initial fluid velocity $\mathbf{u}_0 = \mathbf{0}$, and compare the results obtained by the PKS-NS system with those by the PKS system ($\mathbf{u} \equiv \mathbf{0}$) to explore the influence of the fluid flow on the chemotactic blow-up.

Example 5. *Global existence with $M_\rho \approx 24.67 < 8\pi$.* According to the existence condition of the PKS-NS system in [14], i.e., the total mass of cells M_ρ is strictly less than 8π, we set the initial cell density as

$$\rho(x, y, 0) = 50 \exp\big(-5\big((x-0.5)^2 + (y-0.5)^2\big)\big), \tag{4.5}$$

where the total mass of cells $M_\rho \approx 24.67$ in $\Omega = (0,1) \times (0,1)$. We apply the Fourier-spectral method in space with 128×128 modes, and use the first order Scheme 3.1 ($k = 1$) with $\delta t = 10^{-3}$ to solve the PKS-NS system. Maxima of ρ of the PKS system and PKS-NS system are shown in Fig. 7. It is clear that the two maxima of ρ gradually decrease and reach their steady states almost simultaneously. Fig. 8 displays evolutions of min ρ, mass of ρ, total energy E_{tot}, and kinetic energy of the PKS-NS system. We observe that the value of ρ remains non-negative, the mass of ρ is preserved, and the total

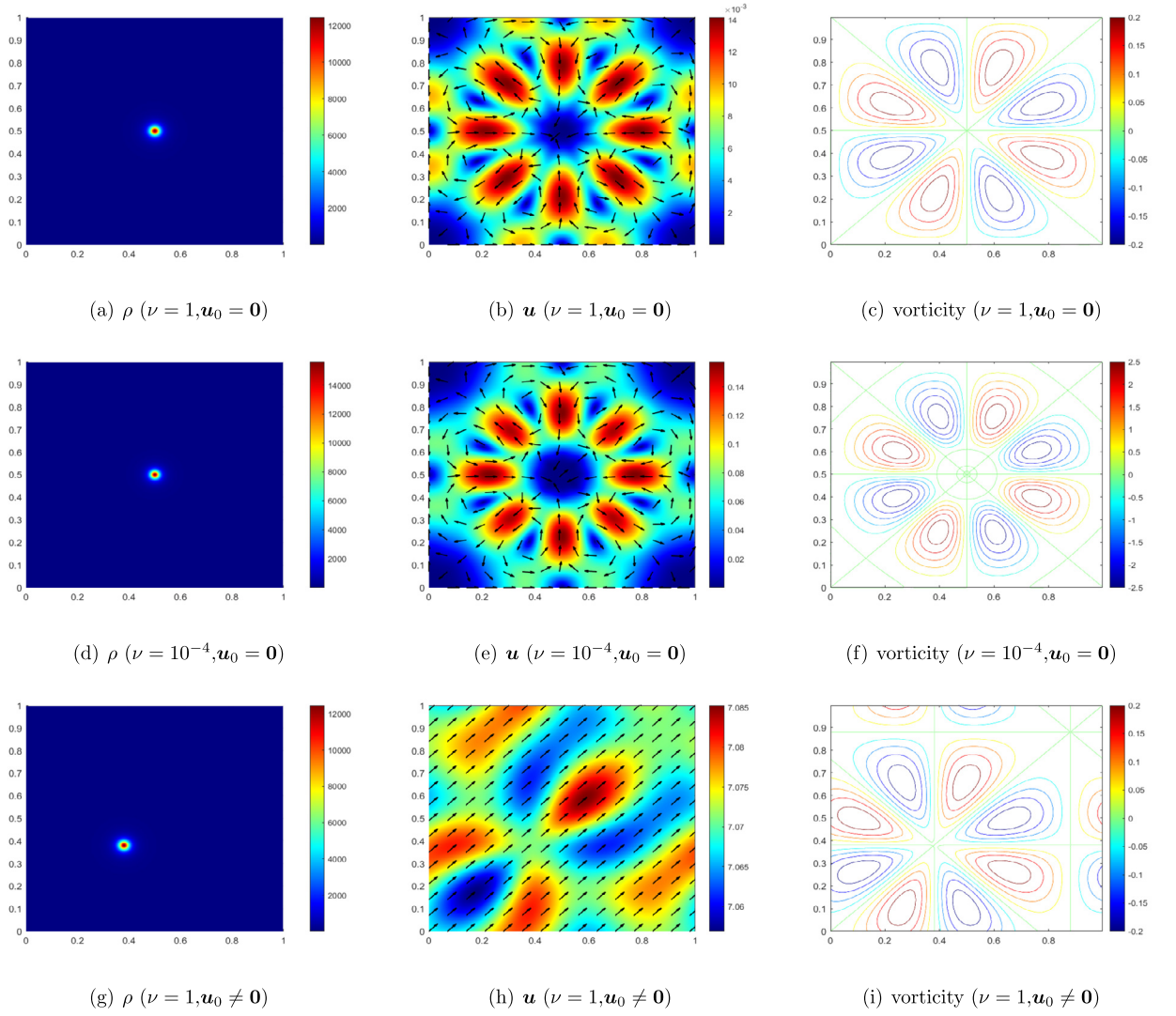

(a) ρ $(\nu = 1, \boldsymbol{u}_0 = \mathbf{0})$ (b) $\boldsymbol{u}$ $(\nu = 1, \boldsymbol{u}_0 = \mathbf{0})$ (c) vorticity $(\nu = 1, \boldsymbol{u}_0 = \mathbf{0})$

(d) ρ $(\nu = 10^{-4}, \boldsymbol{u}_0 = \mathbf{0})$ (e) $\boldsymbol{u}$ $(\nu = 10^{-4}, \boldsymbol{u}_0 = \mathbf{0})$ (f) vorticity $(\nu = 10^{-4}, \boldsymbol{u}_0 = \mathbf{0})$

(g) ρ $(\nu = 1, \boldsymbol{u}_0 \neq \mathbf{0})$ (h) $\boldsymbol{u}$ $(\nu = 1, \boldsymbol{u}_0 \neq \mathbf{0})$ (i) vorticity $(\nu = 1, \boldsymbol{u}_0 \neq \mathbf{0})$

Fig. 17. Example 8: The cell density ρ, fluid velocity $\mathbf{u}$, and vorticity contours of the PKS-NS system with different ν and $\boldsymbol{u}_0$ at $t = 0.176$.

energy is dissipative, the kinetic energy fluctuates for a short period of time initially but quickly becomes stable. Snapshots of the cell density ρ, fluid velocity $\mathbf{u}$ and vorticity contours are shown in Fig. 9, and the fluid flux $\rho\mathbf{u}$, chemotactic flux $-\nabla\rho + \rho\nabla c$ and total flux $\rho\mathbf{u} - \nabla\rho + \rho\nabla c$ are shown in Fig. 10.

Example 6. *Blow-up with* $M_\rho \approx 27.23 > 8\pi$. In order to explore the chemotactic blow-up, we increase the total mass of cell density to $M_\rho \approx 27.23$ by changing the initial cell density as

$$\rho(x, y, 0) = 130 \exp\big(-15(x^2 + y^2)\big) \tag{4.6}$$

in the domain $\Omega = (-1, 1) \times (-1, 1)$. To ensure the reliability of the numerical results, we refine the mesh with 500×500 modes. We use the first order Scheme 3.1 $(k = 1)$ with $\delta t = 10^{-5}$.

We observe in Fig. 11 that maxima of ρ of the PKS-NS system and PKS system both increase continuously, and eventually blow up in finite time. The blow-up process of the PKS-NS system is very similar to that of the PKS system in the sense that evolutions of their cell density maxima are similar. As pointed in [35], "in the radially symmetric class, the PKS-NS system is decoupled which can be seen from the dynamics of the second moment and PKS system itself can develop finite time singularities in the case $M_\rho > 8\pi$". We recall that the numerical result in [33] indicated that solutions to a PKS-Stokes model did not blow-up with initial mass $M_\rho \approx 27$.

Moreover, we observe in Fig. 12 that the positivity of ρ is preserved, the mass of ρ is conserved, and the total energy is dissipative in the whole process, the kinetic energy fluctuates greatly but at very small magnitude.

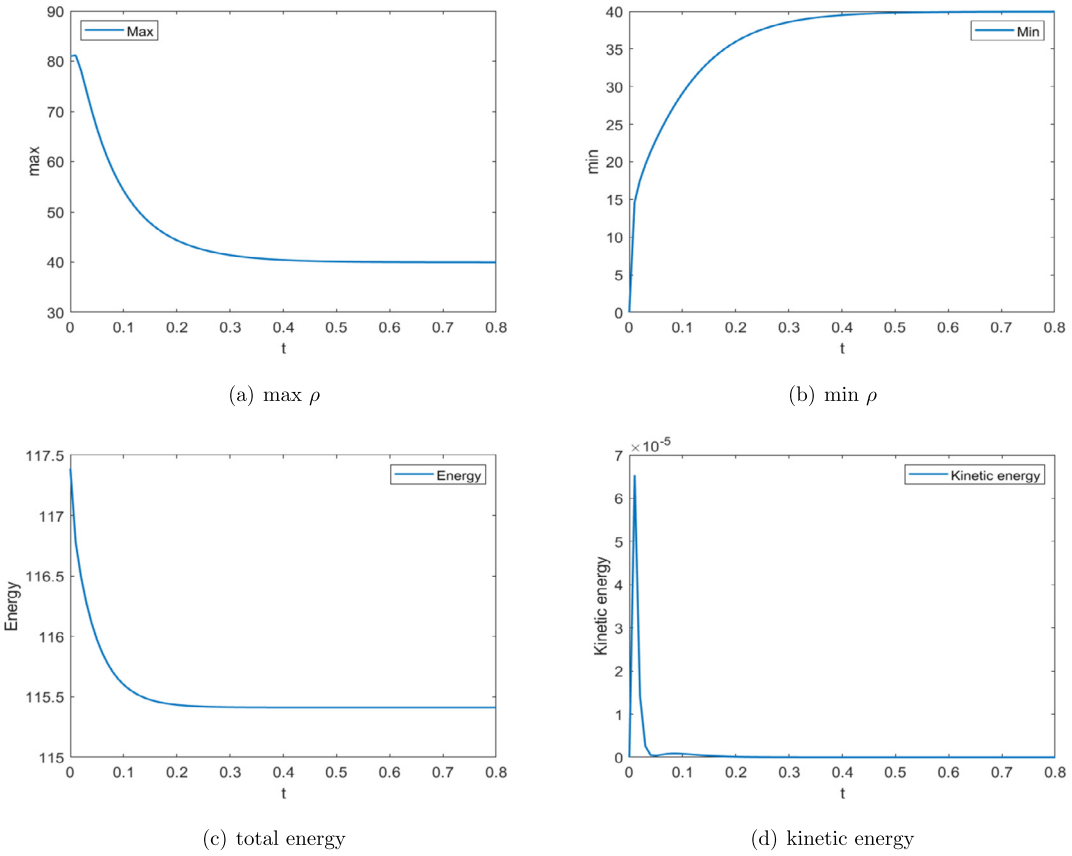

(a) max ρ (b) min ρ

(c) total energy (d) kinetic energy

Fig. 18. Example 9: Evolutions of max ρ, min ρ, total energy E_{tot}, and kinetic energy of the PKS-NS system with $\eta(\rho) = \frac{\rho}{1+\kappa\rho}$.

Example 7. *Blow-up with $M_\rho \approx 39.96 > 8\pi$.* Next we study the blow-up with a larger M_ρ by setting the initial cell density to

$$\rho(x, y, 0) = 81 \exp\big(-5\big((x-0.5)^2 + (y-0.5)^2\big)\big) \tag{4.7}$$

in the domain $\Omega = (0, 1) \times (0, 1)$. We use the Fourier-spectral method in space with 400×400 modes, and the third order Scheme 3.1 ($k = 3$) with $\delta t = 10^{-5}$. Fig. 13 indicates that, for both PKS system and PKS-NS system, the magnitude of max ρ increases rapidly after an initial time interval, and blows up in finite time. Fig. 14 (a)-(c) reveal that the cell density ρ accumulates toward the center as time increases. Distributions of fluid velocity $\mathbf{u}$, and vorticity contours are displayed in Fig. 14 (d)-(f) and (g)-(i), and the fluid flux $\rho\mathbf{u}$, chemotactic flux $-\nabla\rho + \rho\nabla c$ and total flux $\rho\mathbf{u} - \nabla\rho + \rho\nabla c$ are shown in Fig. 15.

Example 8. *The influence of the viscosity and initial fluid velocity on the blow-up.* First, we compare the results with viscosity coefficient $\nu = 1, 10^{-4}$, but keep other parameters the same as those in Example 7. Fig. 16 shows evolutions of max ρ and kinetic energy of the PKS-NS system with different parameters. We find that when the viscosity coefficient of the fluid is changed from $\nu = 1$ to $\nu = 10^{-4}$, the kinetic energy has increased and its evolution form has changed. But there is no significant effect on blow-up by the change of viscosity. Fig. 17 displays the cell density ρ, fluid velocity $\mathbf{u}$, and vorticity contours of the PKS-NS system with different parameters at $t = 0.176$. We observe that the small viscosity increases the fluid velocity and makes the fluid more chaos, but has little effect on the chemotactic blow-up.

Next, we increase the initial fluid velocity to $\boldsymbol{u}_0 = (5; 5)$, but keep other conditions the same as those in Example 7. We observe in Fig. 16 that when the initial fluid velocity is changed from $\boldsymbol{u}_0 = (0; 0)$ to $\boldsymbol{u}_0 = (5; 5)$, the kinetic energy has increased significantly, while the evolution form has hardly changed. In addition, the evolution of max ρ also has hardly changed. However, the concentration point of the cell density shifts from the center of the area due to the given initial fluid velocity.

Example 9. *Prevention of blow-up with $\eta(\rho) = \frac{\rho}{1+\kappa\rho}$.* In this example, we investigate whether a concentration-dependent mobility would prevent blow-up. We set $\eta(\rho) = \frac{\rho}{1+\kappa\rho}$ and $\kappa = 0.01$ for the PKS-NS system, but keep other parameters

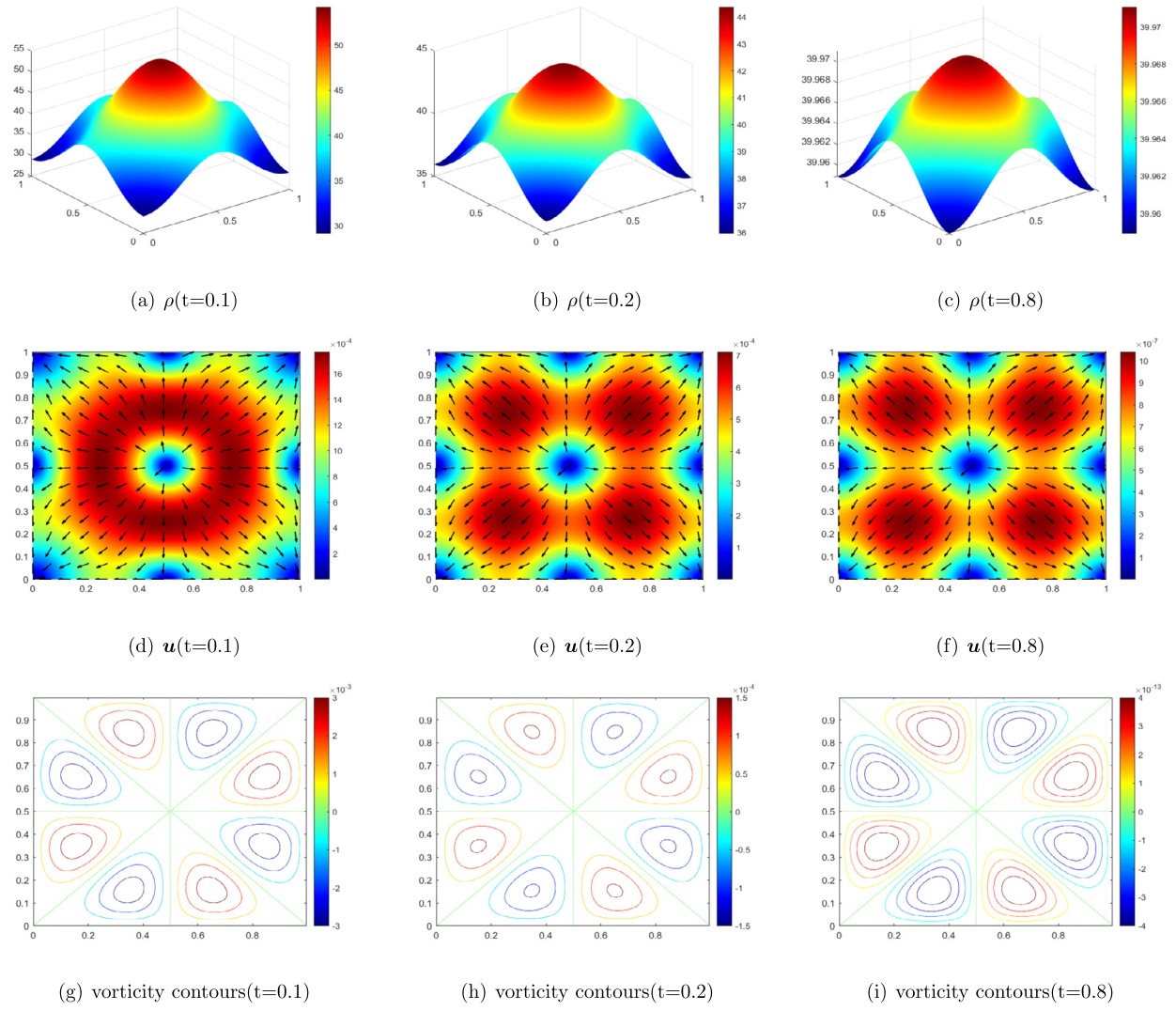

(a) ρ(t=0.1) (b) ρ(t=0.2) (c) ρ(t=0.8)

(d) $\boldsymbol{u}$(t=0.1) (e) $\boldsymbol{u}$(t=0.2) (f) $\boldsymbol{u}$(t=0.8)

(g) vorticity contours(t=0.1) (h) vorticity contours(t=0.2) (i) vorticity contours(t=0.8)

Fig. 19. Example 9: Snapshots of the cell density ρ, fluid velocity $\mathbf{u}$, and vorticity contours of the PKS-NS system with $\eta(\rho) = \frac{\rho}{1+\kappa\rho}$.

the same as those in Example 7. We use the Fourier-spectral method in space with 300×300 modes, and the first order Scheme 3.1 ($k = 1$) with $\delta t = 10^{-4}$ to solve this PKS-NS system.

Evolutions of max ρ, min ρ, total energy E_{tot} and kinetic energy are presented in Fig. 18. It indicates that the maximum of ρ keeps decreasing until it reaches a steady state. Additionally, the positivity of ρ is preserved, and the total energy is dissipative. Fig. 19 shows snapshots of the cell density ρ, fluid velocity $\mathbf{u}$, and vorticity contours. We observe that there is no chemotactic accumulation for cells. In other words, the blow-up in Example 7 is prevented with a concentration-dependent mobility.

5. Concluding remarks

We developed in this paper a class of efficient and accurate semi-discrete-in-time schemes for the PKS-NS system. These schemes enjoy the following remarkable features:

- bound/positivity preserving for the cell density through a suitable function transform;
- fully decoupled and require only solving a sequence of linear equations with constant coefficients;
- unconditional energy dissipation with a modified energy and mass conservation;
- can be higher-order accurate; and
- can be combined with any consist Galerkin-type discretization in space.

We carried out a host of numerical tests to validate our schemes, and simulated the chemotactic non-aggregation and aggregation with a saturation concentration, and investigated blow-up phenomena of the PKS-NS system. Our numerical tests indicate that solutions to the PKS-NS system globally exist when the total mass of cells M_ρ is strictly less than 8π, and can blow up in finite time when $M_\rho > 8\pi$. Besides, the blow-up phenomenon is very similar to that of the PKS system without flow in the sense that evolutions of their cell density maxima are similar. On the other hand, the blow-up of the PKS-NS system can be prevented with a concentration-dependent mobility function $\eta(\rho)$. Our numerical results also indicate that smaller viscosity and larger initial velocity did not have much effect on the blow-up, at least for the parameter ranges that we simulated. However, whether the blow-up would be suppressed with even stronger fluid flow requires further investigation.

CRediT authorship contribution statement

All authors have contributed equally on this paper.

Declaration of competing interest

The authors declare that they have no known competing financial interests or personal relationships that could have appeared to influence the work reported in this paper.

Data availability

No data was used for the research described in the article.

References

[1] L. Almeida, F. Bubba, B. Perthame, C. Pouchol, Energy and implicit discretization of the Fokker-Planck and Keller-Segel type equations, Netw. Heterog. Media 14 (1) (2019) 23–41.
[2] G. Arumugam, J. Tyagi, Keller-Segel chemotaxis models: a review, Acta Appl. Math. 171 (1) (2021) 1–82.
[3] J.P. Boyd, Chebyshev and Fourier Spectral Methods, 2001, New York.
[4] A. Blanchet, J. Dolbeault, B. Perthame, Two-dimensional Keller-Segel model: optimal critical mass and qualitative properties of the solutions, Electron. J. Differ. Equ. 44 (2006) 1–32.
[5] J. Bedrossian, S. He, Suppression of blow-up in Patlak-Keller-Segel via shear flows, SIAM J. Math. Anal. 49 (6) (2017) 4722–4766.
[6] A. Chertock, A. Kurganov, A second-order positivity preserving central-upwind scheme for chemotaxis and haptotaxis models, Numer. Math. 111 (2) (2008) 169–205.
[7] M. Chae, K. Kang, J. Lee, Existence of smooth solutions to coupled chemotaxis-fluid equations, Discrete Contin. Dyn. Syst. 33 (6) (2013) 2271–2297.
[8] A. Chertock, K. Fellner, A. Kurganov, A. Lorz, P.A. Markowich, Sinking, merging and stationary plumes in a coupled chemotaxis-fluid model: a high-resolution numerical approach, J. Fluid Mech. 694 (2012) 155–190.
[9] W. Chen, Q. Liu, J. Shen, Error estimates and blow-up analysis of a finite-element approximation for the parabolic-elliptic Keller-Segel system, Int. J. Numer. Anal. Model. 19 (2022) 275–298.
[10] G. Chamoun, M. Saad, R. Talhouk, Numerical analysis of a chemotaxis-swimming bacteria model on a general triangular mesh, Appl. Numer. Math. 127 (2018) 324–348.
[11] Y. Deleuze, C.Y. Chiang, M. Thiriet, T.W. Sheu, Numerical study of plume patterns in a chemotaxis-diffusion-convection coupling system, Comput. Fluids 126 (2016) 58–70.
[12] Y. Dolak, C. Schmeiser, The Keller-Segel model with logistic sensitivity function and small diffusivity, SIAM J. Appl. Math. 66 (1) (2005) 286–308.
[13] S. Ghorai, N.A. Hill, Periodic arrays of gyrotactic plumes in bioconvection, Phys. Fluids 12 (1) (2000) 5–22.
[14] Y. Gong, S. He, On the 8π-critical-mass threshold of a Patlak-Keller-Segel-Navier-Stokes system, SIAM J. Math. Anal. 53 (3) (2021) 2925–2956.
[15] J.L. Guermond, J. Shen, A new class of truly consistent splitting schemes for incompressible flows, J. Comput. Phys. 192 (1) (2003) 262–276.
[16] D. Horstmann, From 1970 until present: the Keller-Segel model in chemotaxis and its consequences I, Jahresber. Dtsch. Math.-Ver. 105 (3) (2003) 103–165.
[17] S. He, Suppression of blow-up in parabolic-parabolic Patlak-Keller-Segel via strictly monotone shear flows, Nonlinearity 31 (8) (2018) 3651–3688.
[18] M.M. Hopkins, L.J. Fauci, A computational model of the collective fluid dynamics of motile micro-organisms, J. Fluid Mech. 455 (2002) 149–174.
[19] X. Huang, X. Feng, X. Xiao, K. Wang, Fully decoupled, linear and positivity-preserving scheme for the chemotaxis-Stokes equations, Comput. Methods Appl. Mech. Eng. 383 (2) (2021) 113909.
[20] T. Hillen, K.J. Painter, Global existence for a parabolic chemotaxis model with prevention of overcrowding, Adv. Appl. Math. 26 (4) (2001) 280–301.
[21] T. Hillen, K.J. Painter, A user's guide to PDE models for chemotaxis, J. Math. Biol. 58 (1–2) (2009) 183–217.
[22] A.J. Hillesdon, T.J. Pedley, O. Kessler, The development of concentration gradients in a suspension of chemotactic bacteria, Bull. Math. Biol. 57 (2) (1995) 299–344.
[23] F. Huang, J. Shen, Bound/positivity preserving and energy stable SAV schemes for dissipative systems: applications to Keller-Segel and Poisson-Nernst-Planck equations, SIAM J. Sci. Comput. 43 (3) (2021).
[24] F. Huang, J. Shen, Stability and error analysis of a class of high-order IMEX schemes for Navier-Stokes equations with periodic boundary conditions, SIAM J. Numer. Anal. 59 (6) (2021) 2926–2954.
[25] F. Huang, J. Shen, A new class of implicit-explicit BDFk SAV schemes for general dissipative systems and their error analysis, Comput. Methods Appl. Mech. Eng. 392 (2022) 114718.
[26] M. Jiang, Z. Zhang, J. Zhao, Improving the accuracy and consistency of the scalar auxiliary variable (SAV) method with relaxation, J. Comput. Phys. 456 (2022) 110954.
[27] W. Jäger, S. Luckhaus, On explosions of solutions to a system of partial differential equations modelling chemotaxis, Trans. Am. Math. Soc. 329 (2) (1992) 819–824.
[28] H. Kozono, M. Miura, Y. Sugiyama, Existence and uniqueness theorem on mild solutions to the Keller-Segel system coupled with the Navier-Stokes fluid, J. Funct. Anal. 270 (5) (2016) 1663–1683.

[29] H. Kozono, M. Miura, Y. Sugiyama, Time global existence and finite time blow-up criterion for solutions to the Keller-Segel system coupled with the Navier-Stokes fluid, J. Differ. Equ. 267 (9) (2019) 5410–5492.
[30] E.F. Keller, L.A. Segel, Model for chemotaxis, J. Theor. Biol. 30 (2) (1971) 225–234.
[31] A. Kiselev, X. Xu, Suppression of chemotactic explosion by mixing, Archive for Rational Mechanics and Analysis 222 (2) (2016) 1077–1112.
[32] A. Lorz, Coupled chemotaxis fluid model, Math. Models Methods Appl. Sci. 20 (6) (2010) 987–1004.
[33] A. Lorz, A coupled Keller-Segel-Stokes model: global existence for small initial data and blow-up delay, Commun. Math. Sci. 10 (2012) 555–574.
[34] H.G. Lee, J. Kim, Numerical investigation of falling bacterial plumes caused by bioconvection in a three-dimensional chamber, Eur. J. Mech. B, Fluids 52 (2015) 120–130.
[35] C. Lai, J. Wei, Y. Zhou, Global existence of free-energy solutions to the 2D Patlak-Keller-Segel-Navier-Stokes system with critical and subcritical mass, arXiv preprint, arXiv:2101.08306, 2021.
[36] T. Nagai, Blowup of nonradial solutions to parabolic-elliptic systems modeling chemotaxis in two-dimensional domains, J. Inequal. Appl. 6 (2001) 37–55.
[37] C.S. Patlak, Random walk with persistence and external bias, Bull. Math. Biophys. 15 (3) (1953) 311–338.
[38] J. Shen, Efficient spectral-Galerkin method I. Direct solvers of second- and fourth-order equations using Legendre polynomials, SIAM J. Sci. Comput. 15 (6) (1994) 1489–1505.
[39] J. Shen, J. Xu, Unconditionally bound preserving and energy dissipative schemes for a class of Keller-Segel equations, SIAM J. Numer. Anal. 58 (3) (2020) 1674–1695.
[40] R. Temam, Navier-Stokes Equations: Theory and Numerical Analysis, Studies in Mathematics and Its Applications, Amsterdam, 1984.
[41] I. Tuval, L. Cisneros, C. Dombrowski, C.W. Wolgemuth, J.O. Kessler, R.E. Goldstein, Bacterial swimming and oxygen transport near contact lines, Proc. Natl. Acad. Sci. 102 (7) (2005) 2277–2282.
[42] J.L. Velázquez, Point dynamics in a singular limit of the Keller-Segel model 1: motion of the concentration regions, SIAM J. Appl. Math. 64 (4) (2004) 1198–1223.
[43] J.L. Velázquez, Point dynamics in a singular limit of the Keller-Segel model 2: formation of the concentration regions, SIAM J. Appl. Math. 64 (4) (2004) 1224–1248.
[44] M. Winkler, Global large-data solutions in a chemotaxis-(Navier-)-Stokes system modelling cellular swimming in fluid drops, Commun. Partial Differ. Equ. 37 (2) (2012) 319–351.
[45] K. Wu, F. Huang, J. Shen, A new class of higher-order decoupled schemes for the incompressible Navier-Stokes equations and applications to rotating dynamics, J. Comput. Phys. 458 (2022) 111097.
[46] J. Zhao, A revisit of the energy quadratization method with a relaxation technique, Appl. Math. Lett. 120 (2021) 107331.
[47] G. Zhou, N. Saito, Finite volume methods for a Keller-Segel system: discrete energy, error estimates and numerical blow-up analysis, Numer. Math. 135 (1) (2016) 1–47.
[48] Y. Zhang, J. Shen, A generalized SAV approach with relaxation for dissipative systems, J. Comput. Phys. (2022) 111311.